INVESTIGATING THE EFFECTS OF THE DISC-CORONA PROPERTIES ON THE X-RAY REVERBERATION TIME LAGS IN AGN

KAMONWAN KHANTHASOMBAT

A Thesis Submitted in Partial Fulfillment of the Requirements for the
Degree of Master of Science in Physics
Suranaree University of Technology
Academic Year 2023

การศึกษาคุณสมบัติของระบบจานพอกพูนมวลและโคโรนา ที่มีผลต่อความหน่วงเวลาในการสะท้อนของรังสีเอกซ์ บริเวณนิวเคลียสดาราจักรกัมมันต์

นางสาวกมลวรรณ ขันธสมบัติ

วิทยานิพนธ์นี้เป็นส่วนหนึ่งของการศึกษาตามหลักสูตรวิทยาศาสตรมหาบัณฑิต

สาขาวิชาฟิสิกส์

มหาวิทยาลัยเทคโนโลยีสุรนารี

ปีการศึกษา 2566

INVESTIGATING THE EFFECTS OF THE DISC-CORONA PROPERTIES

ON THE X-RAY REVERBERATION TIME LAGS IN AGN

Suranaree University of Technology has approved this thesis submitted in partial fulfillment of the requirements for a Master's Degree.

Thesis Examining Committee

Wasutep Luangtip

(Asst. Prof. Dr. Wasutep Luangtip)

Chairperson

Poemwai Chainakun.

(Assoc. Prof. Dr. Poemwai Chainakun)

Member (Thesis Advisor)

(Asst. Prof. Dr. Tirawut Worrakitpoonpon)

Member

(Asst. Prof. Dr. Ittipon Fongkaew)

Member

(Assoc. Prof. Dr. Yupaporn Ruksakulpiwat)

Vice Rector for Academic Affairs

and Quality Assurance

(Prof. Dr. Santi Maensiri)

Dean of Institute of Science

กมลวรรณ ขันธสมบัติ : การศึกษาคุณสมบัติของระบบจานพอกพูนมวลและโคโรนาที่มีผลต่อความหน่วงเวลาในการสะท้อนของรังสีเอกซ์บริเวณนิวเคลียสดาราจักรกัมมันต์ (INVESTIGATING THE EFFECTS OF THE DISC-CORONA PROPERTIES ON THE X-RAY REVERBERATION TIME LAGS IN AGN) อาจารย์ที่ปรึกษา : รองศาสตราจารย์ ดร.เพิ่มวัย ชัยนะกุล, 57 หน้า.

คำสำคัญ: นิวเคลียสดาราจักรกัมมันต์, จานพอกพูนมวล, โคโรนา, หลุมดำ

วิทยานิพนธ์ฉบับนี้จัดทำขึ้นเพื่อวิเคราะห์และเปรียบเทียบผลของการใช้แบบจำลองความหน่วงเวลาการสะท้อน `KYNxilrev` และ `KYNrefrev` ซึ่งจำลองการสะท้อนของรังสีเอกซ์โดยอาศัยแบบจำลอง `xillver` และ `reflionx` ในการศึกษาระบบของจานพอกพูนมวลและโคโรนาบริเวณนิวเคลียสดาราจักรกัมมันต์ การวิเคราะห์ความสัมพันธ์ระหว่างค่าความหน่วงเวลาของรังสีเอกซ์ (X-ray reverberation lag, τ) และตัวแปรต่าง ๆ ที่ใช้การอธิบายลักษณะของระบบ ได้แก่ มวลของหลุมดำบริเวณใจกลางระบบ (M_{BH}) มุมเอียงของระบบ (i) ตำแหน่งความสูงของโคโรนา (h) ค่าโฟตอนอินเดกซ์ของรังสีเอกซ์จากโคโรนา (Γ) และกำลังส่องสว่างของนิวเคลียสดาราจักรกัมมันต์ (L) พบว่าแบบจำลองทั้ง `KYNxilrev` และ `KYNrefrev` ให้ผลที่สอดคล้องกัน คือ ตำแหน่งความสูงของโคโรนา (h) นั้นมีความสัมพันธ์ทั้งกับค่าความหน่วงเวลา (τ) และมวลของหลุมดำ (M_{BH}) โดยความสูงของโคโรนามีแนวโน้มที่จะลดลงในระบบของหลุมดำมวลน้อย ซึ่งมีค่าอยู่ในช่วง $h \sim 5$–$15\ r_g$ สำหรับ $M_{BH} \sim 10^5$–$10^9\ M_\odot$ อย่างไรก็ตาม M_{BH} และ h ที่ได้จากแบบจำลอง `KYNxilrev` จะมีค่าน้อยกว่าผลที่ได้จาก `KYNrefrev` ซึ่งสามารถสังเกตเห็นความต่างนี้ได้ชัดขึ้นในระบบของหลุมดำที่มีค่าการหมุน (spin parameter, a) น้อย อีกหนึ่งข้อแตกต่างที่สำคัญ คือ ความสัมพันธ์ระหว่าง h และ L ซึ่งจะมีความเด่นชัดมากกว่าเมื่อใช้ `KYNrefrev` ผลการทดลองทั้งหมดแสดงให้เห็นถึงความแตกต่างเชิงเปรียบเทียบของการเลือกใช้แบบจำลองใด ๆ ในการศึกษาลักษณะของระบบจานพอกพูนมวลบริเวณรอบหลุมดำ

สาขาวิชาฟิสิกส์	ลายมือชื่อนักศึกษา	Kamonwan
ปีการศึกษา 2566	ลายมือชื่ออาจารย์ที่ปรึกษา	Poemwai Chainakul.

KAMONWAN KHANTHASOMBAT : INVESTIGATING THE EFFECTS OF THE DISC-CORONA PROPERTIES ON THE X-RAY REVERBERATION TIME LAGS IN AGN. THESIS ADVISOR : ASSOC. PROF. POEMWAI CHAINAKUN, Ph.D. 57 PP.

Keyword: Active Galactic Nuclei, Accretion disc, Corona, Black hole

In this thesis, we have conducted a comparative study to explore the constrained parameters of active galactic nuclei (AGN) using the public X-ray reverberation models `KYNxilrev` and `KYNrefrev`. These models employ the reflection codes, `xillver` and `reflionx`, to explain the reflection from the accretion disc. The main parameters include the central black hole mass (M_{BH}), coronal height (h), inclination (i), photon index of the continuum emission (Γ), and source luminosity (L). The lag-frequency spectra that explain the time delay between the coronal X-rays and the reflection X-rays from the disc are generated. Our focus is specifically on simulated AGN conforming to the established scaling law between the lag amplitude (τ) and M_{BH}. In our simulated datasets, we demonstrate a correlation between τ and h, suggesting the potential establishment of an independent scaling law. Furthermore, we observe a positive scaling relationship between h (in gravitational units) and M_{BH}, indicating a more compact corona in lower-mass AGN. Both models consistently indicate that the coronal height is likely found within the range of approximately 5–15 gravitational radii (r_g) across low- to high-mass AGN. However, it is noteworthy that `KYNxilrev` suggests lower M_{BH} and h values compared to `KYNrefrev`, with this disparity being more pronounced in lower-spin AGN. The significant correlation between the source height and luminosity that is seen only in `KYNrefrev` implies a potential model-dependent nature of the h–L relationship. Our findings underscore the differences between these public X-ray reverberation models, prompting considerations regarding potential biases in parameter estimates and inferred correlations.

School of Physics
Academic Year 2023

Student's Signature kamonwan
Advisor's Signature Poemwai Chainakun

ACKNOWLEDGEMENTS

Out of my respect, I would like to thank my supervisor, Assoc. Prof. Dr. Poemwai Chainakun, for always valuing my idea and my opinion and for giving me many great advises and suggestions toward improving my work. This work would not have been possible without his effort.

I cannot forget my friends: The one who went through many hard times together, listened and cheered me on and School of Physics colleagues who always willing to help whenever I ask for.

Furthermore, I wish to express gratitude for the financial assistance received through the scholarship provided by the Thai government under the Development and Promotion of Science and Technology Talents Project, administered by the Institute for the Promotion of Teaching Science and Technology (IPST). This funding has been instrumental in facilitating the execution of my research project, enabling me to secure essential resources and advance my academic pursuits.

Kamonwan Khanthasombat

CONTENTS

CONTENTS (Continued)

LIST OF TABLES

Table **Page**

LIST OF FIGURES

LIST OF FIGURES (Continued)

Figure **Page**

LIST OF FIGURES (Continued)

LIST OF ABBREVIATIONS

AGN	Active Galactic Nuclei
M_{BH}	Black hole mass
$M_{\odot}$	Solar mass
c	Speed of light
G	Gravitational constant
r_g	Gravitational radii where $r_g = GM_{\mathrm{BH}}/c^2$
a	Spin parameter
Γ	Photon index
ξ	Ionization parameter
r_s	Spearman's rank order correlation coefficient
L	Luminosity
τ	Time lag
ν	Frequency

CHAPTER I

INTRODUCTION

An Active Galactic Nucleus (AGN) is a central, dynamically influential region in the active galaxies that contains a supermassive black hole and other surrounding elements such as an accretion disc, a corona — a cloud of electron plasma, and a torus. Despite significant advancements, the precise geometry of this system continues to be a subject of active research and debate, with various theoretical models as shown in Figure 1.1. The gravitational force induces the accretion disc to be co-rotated with the central black hole so that the disc gains more energy and emits the photons with energy in the UV/Optical band via the blackbody radiation process (i.e., thermal radiation). However, the observations have shown that the spectra from AGN can be in a wider range of waveband, extending to the hard X-ray and gamma-ray regimes. The crucial physical process that is believed to produce the X-ray photons is the Compton up-scattering of the disc photons with higher energy electrons inside the corona. Generally, the X-ray radiation is likely produced inside the corona at the innermost region around the black hole where the gravitational force is extremely strong (Fabian et al., 2000).

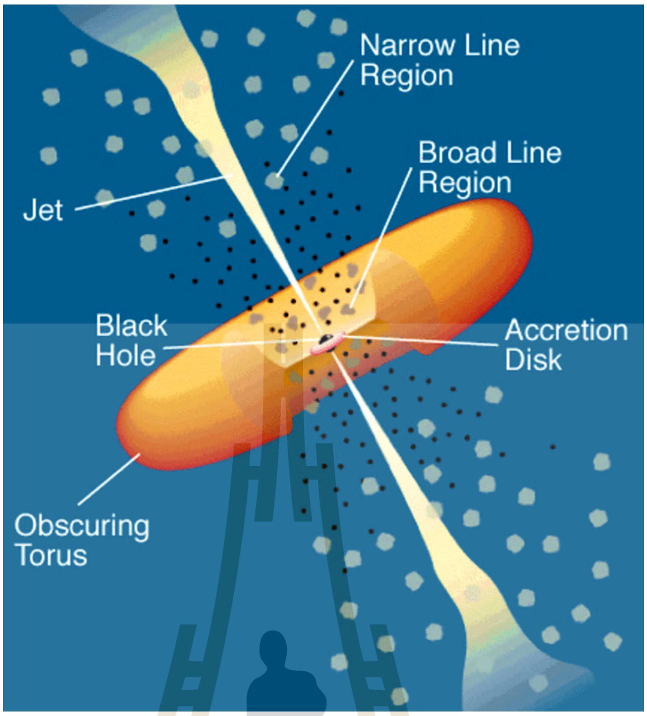

Figure 1.1 The Schematic diagram of the AGN system with the central black supermassive hole, accretion disc and the torus. Figure from Palma et al., 2011.

Observed X-rays from the AGN can be classified into two main components: the primary and reflected spectra. Once emitted from the X-ray corona, some of the up-scattered photons travel to and 'reflect' on the accretion disc instead of traveling directly to the observer (Caballero-García et al., 2018; Kammoun et al., 2021). The reflection of the photons on the disc involves multiple processes, for example, backscattered and fluorescent emission (Fabian and Ross, 2010; Uttley et al., 2014). Since most of the key elements in the AGN system (e.g., the black hole, the accretion disc, and the corona) are relevant in the production of these X-rays, the X-ray spectra are imprinted with the significant features offering indispensable insights into the intrinsic characteristics, structural morphology, and dynamic behavior of the constituent components within the AGN, especially in the disc-corona system (Fabian et al., 1999; Peterson et al., 2004).

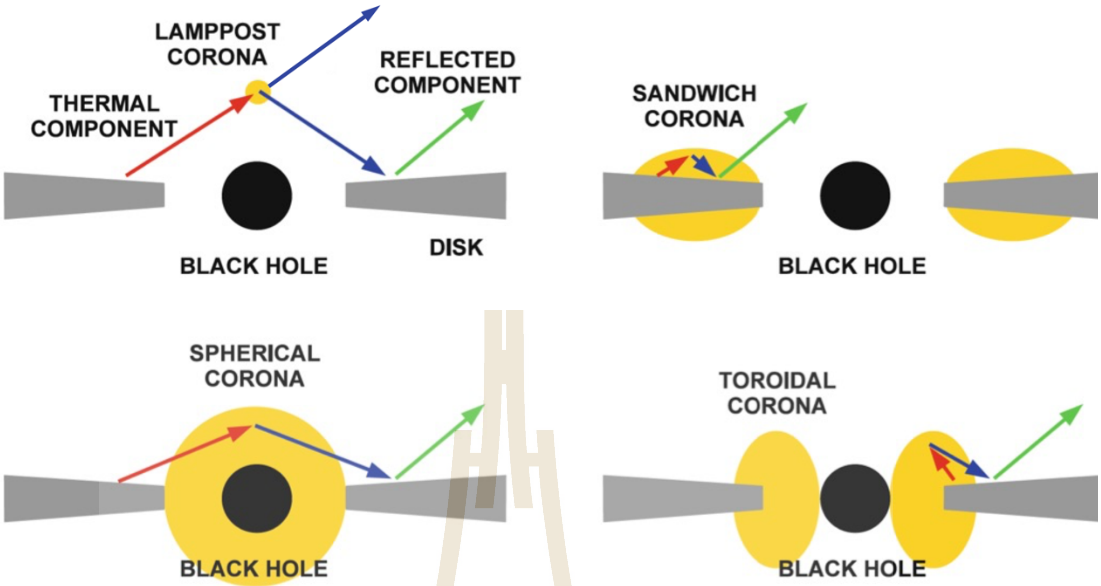

Figure 1.2 The Schematic diagram of the AGN system with the central black supermassive hole, accretion disc and corona. The figure includes the lamp-post model (upper left), slab or sandwich corona model (upper right), spherical corona model (lower left) and toroidal corona model (lower right). The primary and reflected X-rays are shown as the blue and green arrows, respectively. Figure adapted from Bambi et al., 2021.

Besides the time-average spectra, we can investigate the differences in the light-traveling path of the X-rays as seen by an observer. This delay is commonly referred to as the "X-ray reverberation time lag" and its magnitude can be used to constrain the structure and property of various physical elements within the system, such as the size and geometry of the X-ray source, the mass of the black hole, and the inclination angle. The method of using the time lags for such analyses is known as reverberation mapping (Blandford and McKee, 1982; Fabian et al., 2009; Cackett et al., 2014). Notably, not only in the X-rays, but this method can also be done in different energy ranges or wavelengths. For example, optical reverberation mapping is commonly applied to study regions at a greater distance along the accretion disc while

X-ray reverberation is commonly employed to investigate the innermost areas around the black hole, covering distances of roughly hundreds of light seconds. This work then focused on the X-ray reverberation that arises from the X-ray emissions and reflection that mainly occur in the area closest to the event horizon of the central black hole (Fabian et al., 2000; Ross and Fabian, 2005; García and Kallman, 2010; García et al., 2011).

Various calculation routines, geometric assumptions as well as the reverberation models for performing the computer simulation of AGN spectra have been developed for the past decades. Therefore, we are interested in doing the analysis of the well-known reverberation models that was developed as a ready to use coding package under the **`KYNreverb`** project (Dovčiak, Karas, and Yaqoob., 2004; Dovčiak et al., 2004; Caballero-García et al., 2018), **`KYNxilrev`**, to estimate the AGN parameters (e.g., the black hole mass, the position of the corona and the inclination angle) as well as their correlation, that can be implied from the simulated time lags. Moreover, the comparison of the results to the **`KYNrefrev`** model is provided to show the significant differences and the bias that could benefit in the analysis of the results from these different models in the future.

CHAPTER II

LITERATURE REVIEW

2.1 X-rays from the Active Galactic Nuclei (AGN)

The origin of the X-rays from AGN has been believed to be in the innermost region around the central black hole. The X-rays are produced by the inverse Compton scattering (i.e., the Compton up-scattering) of the disc-emitted photons, usually are UV/Optical photons, with the energetic electrons in the corona (Haardt, 1993; Dove et al., 1997; Dauser et al., 2013). The up-scattered photons then reach the X-ray energy. The X-rays from AGN consists of two main components, the primary and reflected X-rays. Certain portions of the coronal X-ray photons, rather than directly reaching the observer (as a primary spectra), can incident upon the accretion disc (Lightman and White, 1988). These incident photons are then reprocessed, involving with various physical mechanisms such as Compton scattering and photoionization, leading to reflected X-ray photons (i.e., the reflected spectra).

While the primary spectra, the photons that travel from the corona to observer directly, are usually modelled by the power-law profile with the cut-off at the high energy of ~ 200–300 keV (García et al., 2013), the reflected spectra, as produced from multiple processes, are composed with three main characteristic features which are: (i) The fluorescent Fe-Kα emission line typically at the rest-frame energy of ~ 6.4 keV produced in the energy releasing process of the iron (Fe) atom in the accretion disc (Fabian et al., 2000). In the observation, as illustrated in Figure. 2.2, the emission line is often seen in a skewed and broadened appearance with the blue peak and an elongated red tail. This distortion occurs due to fact that the disc is rotating, causing the red and blueshift, as well as the Doppler and relativistic effects in the strong gravitational region, as illustrated in Figure 2.1 (George and Fabian, 1991; Reynolds et al., 1999; Fabian et al., 2000). This distinctive broad and skewed Fe-Kα line profile serves as an effective diagnostic tool for ascertaining fundamental properties, such as the inclination and the spin of the black hole within the system (García et al., 2013). (ii) The reflection or Compton hump at ~ 10–30 keV (George and Fabian 1991; Epitropakis et al., 2016). (iii) The soft excess at energy range of approximately 0.3–1 keV (Ross and Fabian, 2005).

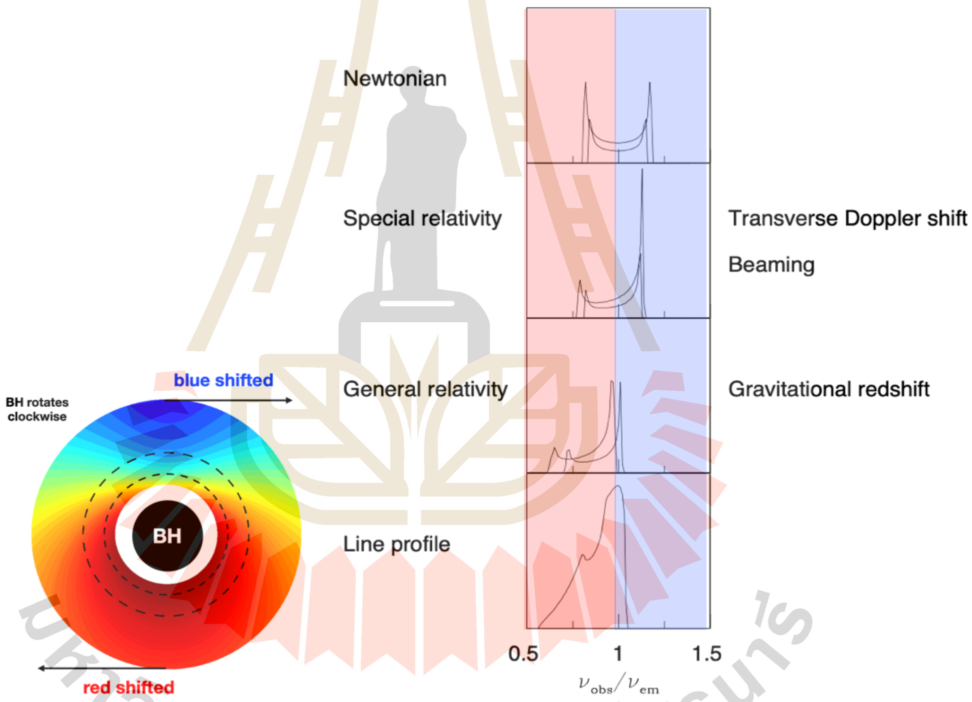

Figure 2.1 The distortion of the emission line by the Newtonian, special relativistic and general relativistic effects. Figure adapted from Fabian et al., 2000.

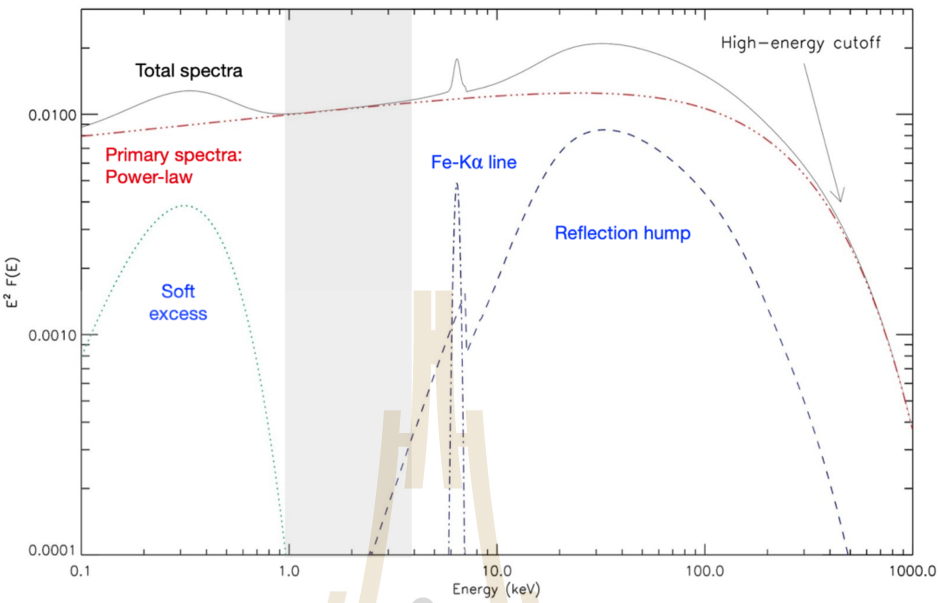

Figure 2.2 The X-rays (0.1–1000 keV) from AGN with the primary and reflected components indicated in red and blue, respectively. The overall shape of the spectra can be found in the solid black line. Figure from Ricci et al., 2011, PhD thesis.

2.2 The X-ray reverberation lags in AGN

The primary and reflected components of the X-rays do not arrive at observer at the same time. This leads to a timing parameter called “time delay” or “reverberation lag” as the reflected photons spends more time along the travelling path compared to the primary photons. The reverberation lags relate to the distance between the X-ray source (i.e., the corona) and the reflector (i.e., the accretion disc), so that it can be used to calculate back into the position of the X-ray corona (Uttley et al., 2014; Cackett et al., 2021). The reverberation time lag can be defined to be either positive or negative. Here, the “negative” means “soft” lag indicating that the lower energy components (~ 0.3–1 keV), which generally are dominated by the reflected spectra of the coronal photons after being scattered on the disc, are lagging those with higher energy (~ 1–4 keV), which is usually dominated by the direct primary spectra (vice versa for the “positive” hard lag).

The calculation of time lag as a function of the Fourier frequency, f, can be done by computing the cross spectrum of the complex conjugate of soft-band light curves, $S^{*}(f)$, and hard-band energy light curves, $H(f)$,

$$C(f) = S^{*}(f)\,H(f)\ . \qquad [1]$$

Then, the Fourier average phase lag ($\phi(f)$) and the Fourier time lag ($\tau(f)$) can be calculated via

$$\phi(f) = \arg\,[C(f)]\ , \qquad [2]$$

and,

$$\tau(f) = \phi(f)\,/\,2\pi f\ . \qquad [3]$$

The time lags are defined in the range of (-π, π). The phase wrapping, due to the specific range of the phase lag, where the lag profile fluctuates around 0 can be seen at $f \geq 1/2\tau$ (Nowak et al., 1999; Chainakun and Young, 2015).

The first significant discovery of X-ray reverberation lags in the AGN 1H 0707–495 was published in Fabian et al., in 2009. The results showed that the softer X-ray band (dominated by reflection) is delayed after the harder band (dominated by continuum) by about 30 seconds, as indicated in Figure 2.3 as the grey dashed line. By assuming the lamp-post model scenario with the black hole mass M_{BH} = 2×10^{6} $M_{\odot}$ (Solar mass, $M_{\odot}$ ~ 1.99×10^{30} kg), this lag can be used to estimate the position of the corona above the black hole's rotational axis. Giving the speed of light (c) for the photons, this difference corresponds to an additional distance of about 9 million kilometers, or 6 r_g (gravitational radii, $r_g = GM_{BH}/c^2$, where G is the gravitational constant).

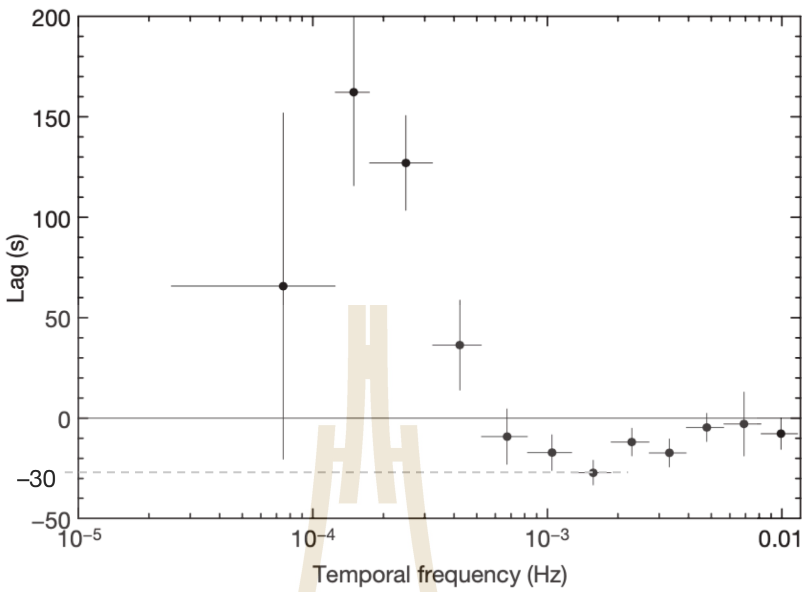

Figure 2.3 The frequency-dependent lags in Fe-L bands (0.3–1 keV vs. 1–4 keV) observed in the AGN 1H 0707–495. Figure adapted from Fabian et al., 2009.

The magnitude of soft lag or "reverberation lag" and its expected frequency were reported to have a significant correlation and anti-correlation respectively with the mass of the central black hole in AGN (De Marco et al., 2013). By investigating 32 sources of the unobscured AGN, the soft lags at high frequencies are presented in 15 out of 32 sources (≥ 97 per cent of significance level). They show the strong correlation with the black hole mass. The plot between the frequency and reverberation lag magnitude and the mass are shown in Figure 2.4. The corresponding equations are

$$\log(|\tau|) = -1.98[\pm 0.08] + 0.59[\pm 0.11] \log(M_{BH}/10^7 M_\odot), \qquad [4]$$

and,

$$\log(\nu_{lag}) = -3.50[\pm 0.07] - 0.47[\pm 0.09] \log(M_{BH}/10^7 M_\odot), \qquad [5]$$

when ν_{lag} is the expected frequency that the negative time lag with magnitude $|\tau|$ was observed. As in Figure 2.4, with increasing black hole mass, the observed lags exhibit a larger magnitude, along with a notable shift of the lag frequencies towards lower Fourier frequencies. The presence of this scaling property in the lags, relative to mass, reinforces the prevailing notion that these reverberation lags primarily originate within the innermost regions of the disc, with their characteristics influenced by the nature of the central compact object. Thereafter, in the work of Mallick et al., (2021) which is the extended investigation from De Marco et al. (2013) by adding more samples with lower mass ($M_{\mathrm{BH}} < 3\times10^{6}\ M_{\odot}$). This scaling relation still hold true. Another work that agrees with this trend is the work of Kara et al. (2016) that performed the analysis on observed lags but in Fe-K bands (2–4 vs. 5–7 keV), as shown in Figure 2.5.

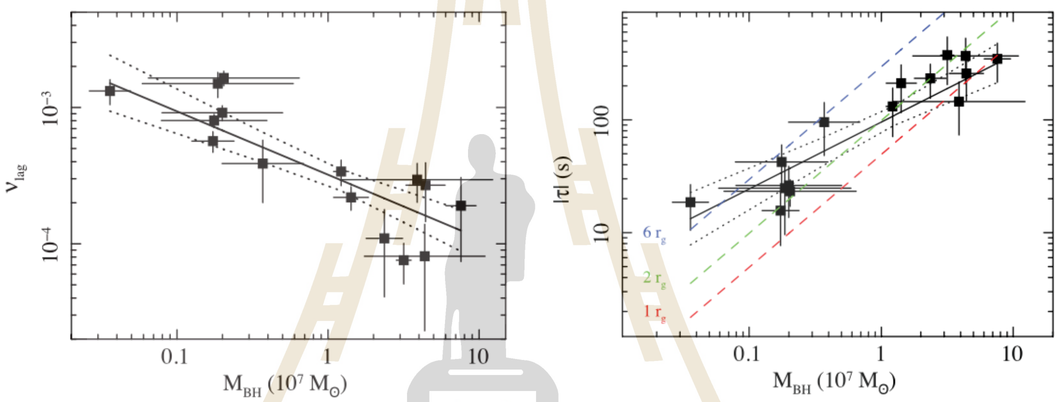

Figure 2.4 Trends of lag magnitude (left panel) and lag frequency (right panel) plotting against the black hole mass of the AGN. The solid lines represent the best-fitting in log-log space. Additionally, the dashed lines in the right-hand panel represent the light-crossing time at 1 r_{g}, 2 r_{g}, and 6 r_{g}. Note that $r_{\mathrm{g}} = GM_{\mathrm{BH}}/c^2$. Figure from De Marco et al., 2013.

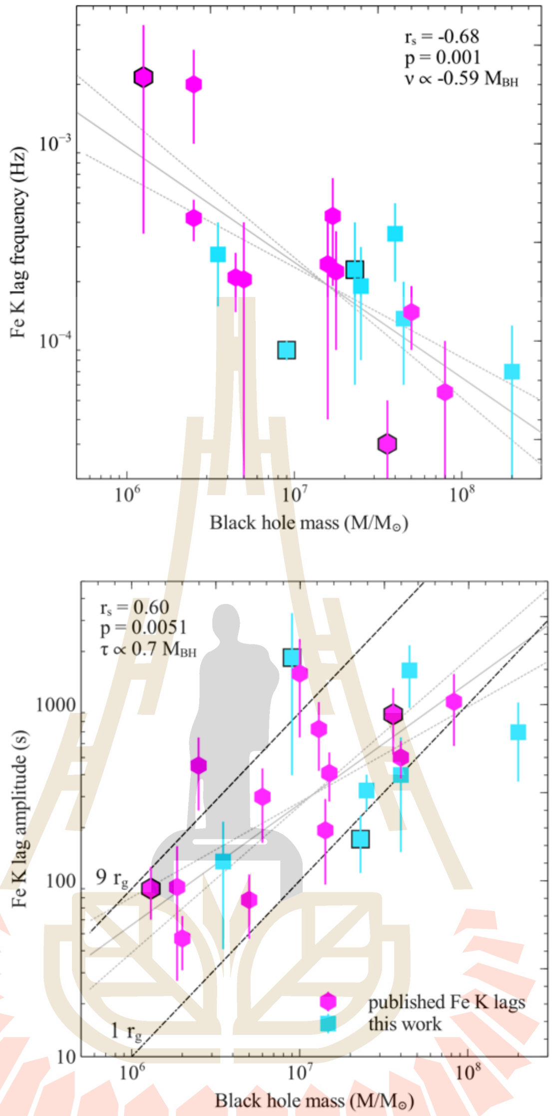

Figure 2.5 Trends of observed Fe-K lag frequency (right panel) and lag magnitude (left panel) plotting against the black hole mass in the AGN system. The grey solid line indicates the best-fitting linear model. The black lines in the lower panel show the time delay for the distance of 1 (dot-dashed line) and 9 r_g (dotted line). Note that the different colors indicate the data that were previously published (pink) and newly published in Kara et al., 2016 (blue). Figure from Kara et al., 2016.

2.3 Public reverberation models and their assumption

Various investigation of the AGN has been done using the computer simulation technique under different assumptions on the disc-corona geometry (Cackett et al., 2014; Emmanoulopoulos et al., 2014; Chainakun and Young, 2015; Chainakun and Young, 2017; Caballero-García et al., 2018; Chainakun et al., 2019; Lucchini et al., 2023), and property of the elements in the system, for example, using different atomic data for the accretion disc. The two well-known models to do the simulation of the AGN X-ray spectra are **`reflionx`** (Ross et al., 1999; Ross and Fabian, 2005) and **`xillver`** (García and Kallman, 2010; García et al., 2013). Also, there are the adapted models based on these two models, such as **`relxill`** and **`xillverRR`**. These models may differ in terms of the atomic data used, which, in most cases, offers different perspectives of the optical process for absorption, excitation, and emission processes (García et al., 2013). The work of García et al., in 2013 shows the comparative analysis of reflected X-ray emission lines between **`reflionx`** and **`xillver`**. Their result is presented in Figure 2.6. Comparing between red (**`reflionx`**) and black (**`xillver`**) lines, especially in energy $\leq$ 1 keV, the **`xillver`** model estimates the less overall spectra compared to those of the **`reflionx`** model. A lower photon index (Γ = 1.4, upper panel) and lower ionization parameter (ξ = 10 erg cm s^{-1}, upper line) produces a large difference between both models. This discrepancy seems to be less noticeable with higher photon index (Γ = 2.6) even when ξ = 10 erg cm s^{-1}, but the difference still presents in the cases of ξ = 1000 erg cm s^{-1}.

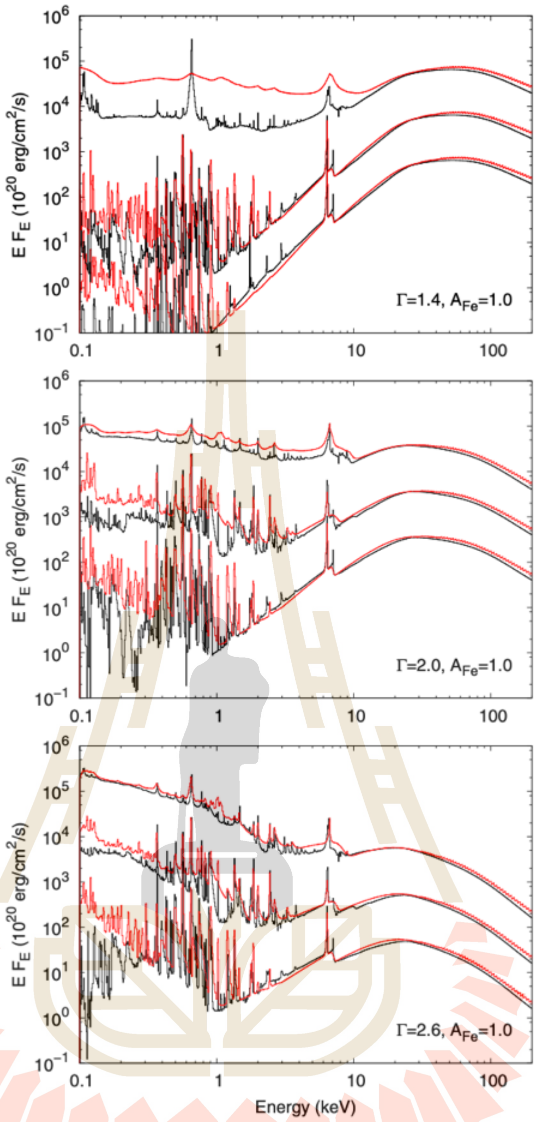

Figure 2.6 The comparison of the simulated reflected X-ray spectra using **`reflionx`** model (red lines) and **`xillver`** model (black lines) with different photon indices of 1.4, 2 and 2.6, from upper to lower panel. In each panel, the ionization parameter was additionally varied to be 10, 100, and 1000 erg cm s^{-1}, shown in lower to upper lines, respectively. Figure from García et al., 2013.

There are multiple papers on AGN parameter analysis using time-lag simulated from different models. The work of Cackett et al., in 2014 revealed the trend of simulated time-lag varying with the coronal height and the inclination angle in Fe-K bands (2–4 vs. 5–7 keV). Note that in this case the reflection is more dominated in 5–7 keV band so the reverberation lags become positive hard lags. The reverberation lags are increased when the on-axis X-ray point source moves higher. The lags are slightly decreased with the smaller inclination angle. Their results are shown in Figure 2.7 and 2.8. The work of Kara et al., in 2016 indicated that there is a correlation between the estimated coronal height and the detected luminosity obtained from the Fe-K hard lags, as shown in Figure 2.9. The assumption that assumed the corona is a point source located on the symmetry axis of the black hole is called the lamp-post model.

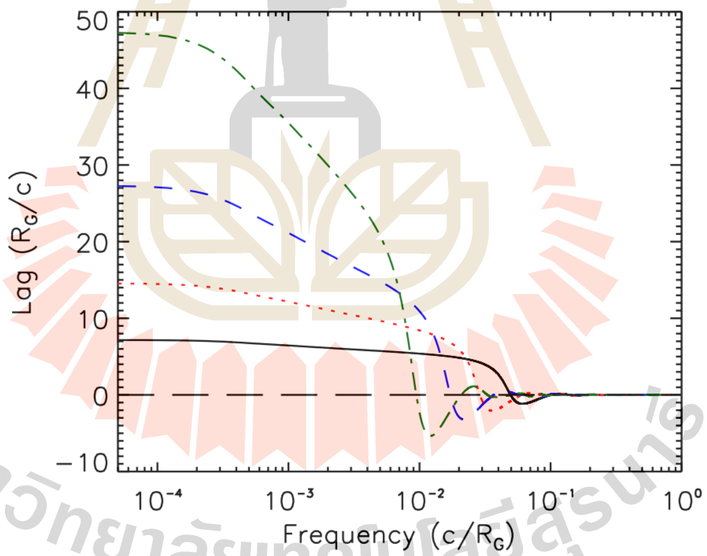

Figure 2.7 Lag-frequency spectra varying with the lamp-post X-ray corona height. The color of the lines indicates the height of 2 r_g (solid black), 5 r_g (dotted red), 10 r_g (dashed blue) and 20 r_g (dashed green). Figure from Cackett et al., 2014.

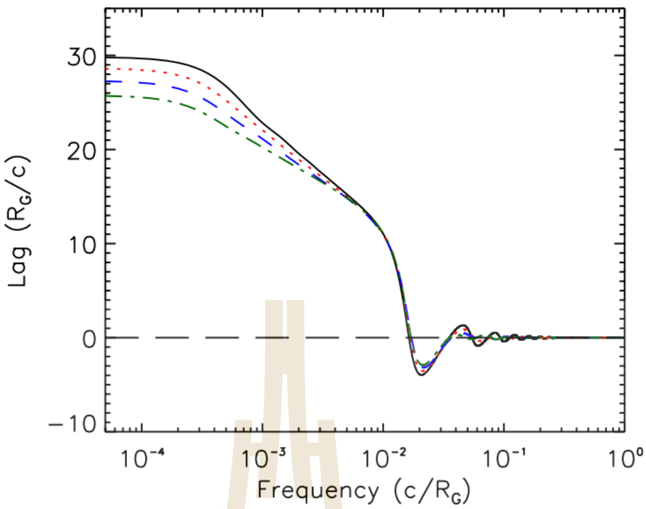

Figure 2.8 Lag-frequency spectra dependent on the inclination angles. The color of the lines indicates the inclination of 5° (solid black), 30° (dotted red), 40° (dashed blue) and 60° (dashed green). Figure from Cackett et al., 2014.

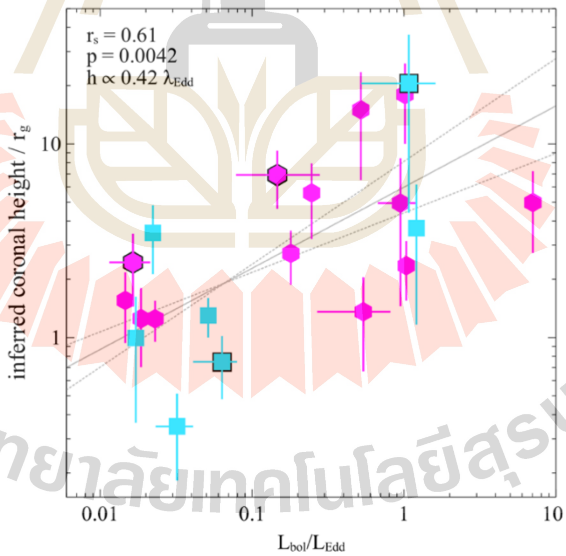

Figure 2.9 The estimated of the corona height and the luminosity in the unit of the Eddington's ratio. The best-fitting model are indicated in grey lines. The Spearman's rank order correlation coefficient (r_s) for the newly published data (plotted in blue) is 0.61 while it is lower (0.41) for the previously published data (plotted in pink). Figure from Kara et al., 2016.

CHAPTER III

METHODOLOGY

This following section is from the manuscript, titled "Parameter dependency on the public X-ray reverberation models **KYNxilrev** and **KYNrefrev**". It was originally included there in section 2 and 3, the "X-ray reverberation models" and "Lag-mass scaling relation and data simulation". The manuscript is now accepted for publication in Monthly Notices of the Royal Astronomical Society (MNRAS) in 2024.

3.1 X-ray reverberation models and AGN parameters

KYNxilrev and **KYNrefrev** is the X-ray reverberation coding model related to the **KYN** package[1] (Dovčiak, Karas, and Yaqoob, 2004; Dovčiak et al., 2004; Caballero-García et al., 2018) that can calculate the frequency-dependent time lags by using the energy-integrated X-ray spectrum from the **xillver** (García and Kallman, 2010; García et al., 2013) and **reflionx** (Ross, Fabian, and Young, 1999; Ross and Fabian, 2005) models. We use **reflionx.mod** as the **reflionx** table model, and specifically employ **xillverD-5.fits** for the **xillver** reflection model

The incident angle of the X-rays irradiating the disc has a significant impact on the rest-frame reflection spectrum. While **reflionx** assumes an isotropic point source situated above a semi-infinite slab of cold gas, **xillver** assumes that the coronal X-rays illuminate the disc with an incident angle of 45 degrees (see, e.g., Dauser et al., 2013 and discussion in Bambi et al., 2021). Furthermore, most of the solar abundances of the elements (e.g., C, O, Ne, Mg and Fe) used in **xillver** are lower than those in

---

[1] http://project.asu.cas.cz/stringgravity/kyn

`reflionx` (García et al., 2013). This is because `reflionx` adopted the elemental solar abundances from Morrison and McCammon (1983), while the `xillver` model calculated the X-ray reprocessing on the accretion disc following the photoionisation routines from XSTAR code (Kallman and Bautista, 2001), which adopted the abundances of the elements from Grevesse and Sauval (1998). Among the widely-utilized reflection models, `xillver` is probably the most sophisticated one. The `XSTAR` code incorporated by `xillver` contains the most comprehensive atomic database for the detailed treatment of the radiative transfer to model photoionized X-ray reflection spectra. `Xillver` also enhances, in particular, the thorough calculation of the K-shell photoabsorption of prominent ions such as N and O (Kallman et al., 2004; García et al., 2005, 2009, 2013; Bambi et al., 2021).

The `KYNxilrev` and `KYNrefrev` models are based on the assumption of the lamp-post coronal geometry (i.e. the corona is an isotropic point source located on the rotational axis of the black hole and produces a flash power-law radiation). The accretion disc is given to be optically thick and geometrically thin that obeys the standard model of Novikov and Thorne (1973). The inner edge of the accretion disc is set to be equivalent to the innermost stable circular orbit (ISCO) while the outer edge is fixed at 1000 r_g. The disc has a constant density profile, while the ionization state of the disc is allowed to vary with the incident flux. The X-ray continuum is given in terms of a cut-off power law with the photon index Γ. The high-energy cut-off is fixed at 300 keV. The frequency-dependent Fe-L lags are calculated using the energy bands of 0.3–0.8 and 1–4 keV. The time lag is computed using the standard Fourier technique (Nowak et al., 1999) mentioned in section 2.2. Furthermore, we set the parameter *xsw* = 16 (default value) in both `KYNxilrev` and `KYNrefrev` models, meaning that the rebinning is done in real and imaginary parts before the lags are computed and further diluted by the primary spectra with respect to the given (observed) energy band.

Table 3.1 List of parameters and the random distribution used in the time lag simulation process. Note that the luminosity is measured in the 2–10 keV energy band.

Parameter	Range (Unit)	Distribution
Black hole mass (M_{BH})	10^5–10^9 $M_{\odot}$	Uniformly in log scale
Coronal height (h)	2–30 r_g	Uniformly in linear scale
Inclination angle (i)	15°–75°	Uniformly in linear scale
Photon index (Γ)	1.8–3.0	Uniformly in linear scale
Luminosity (L)	0.001–0.500 L_{Edd}	Uniformly in log scale

The spin parameter of the black hole, if not stated, is fixed at a = 1. The free parameters investigated here are the black hole mass (M_{BH}), the coronal height (h), the inclination (i), the photon index of the primary continuum (Γ) and the observed 2–10 keV luminosity (L) in the units of the Eddington luminosity (L_{Edd}). We vary M_{BH} in the range of 10^5–10^9 $M_{\odot}$, which also covers the low mass AGN as investigated in Mallick et al., (2021). The coronal height h is varied in the range of 2–30 r_g, while the inclination i is between 15°–75°. The photon index Γ and the luminosity L are varied between 1.8–3.0 and 0.001–0.5 L_{Edd}, respectively. These parameter ranges are presented in Table 3.1. Note that we focus on the case when the inner disc is fixed at ISCO, but we also try to vary the inner radius (the result is presented in Appendix A). The `rand()` is used to generate the random integer with the seed generated by `srand(time(0))` so that it returns a different sequence of random numbers each time it is executed.

3.2 AGN data selection

The studies on the observational surveys of the reverberation lags revealed that the AGN with a higher mass seems to exhibit larger reverberation lags while the observed frequencies of the lags are lower (e.g. De Marco et al., 2013; Kara et al., 2016; Hancock, Young, and Chainakun, 2022). Here, the lag-frequency spectra in the Fe-L band of the mock AGN samples are generated using the **KYNxilrev** and **KYNrefrev** models, by varying the parameters shown in Table 3.1. The examples of the lag-frequency spectra simulated from both models are presented in Figure 3.1. The negative lags are defined as the soft band lagging behind the hard band. As expected, the maximum amplitude of the lag increases with the coronal height. The phase wrapping also occurs at lower frequencies for higher source height. Furthermore, it can be seen that the phase-wrapping frequencies from both models are quite consistent, but, for each source height, the lag amplitude of the **KYNxilrev** model is smaller than that from the **KYNrefrev**. This is expected since the reflection spectrum from the **xillver** model is more absorbed at low energies (García et al., 2013), so the soft lags from the **KYNxilrev** is more diluted than the **KYNrefrev** model. The dilution effects reduce the amplitude of the lags without affecting the phase wrapping (see Wilkins and Fabian, 2013; Kara et al., 2014; Chainakun et al., 2023, for discussion on intrinsic lags and dilution).

From the mass-scaling law, we know the lag amplitude (τ_{obs}) and the particular frequency (ν_{obs}) at which we expect to see the lags for a given black hole mass. Therefore, the simulated lag spectra are screened in order to check if they are consistent with the mass-scaling law suggested by De Marco et al., 2023. The scaling equations are shown as eq. [4] and [5] in section 2.2.

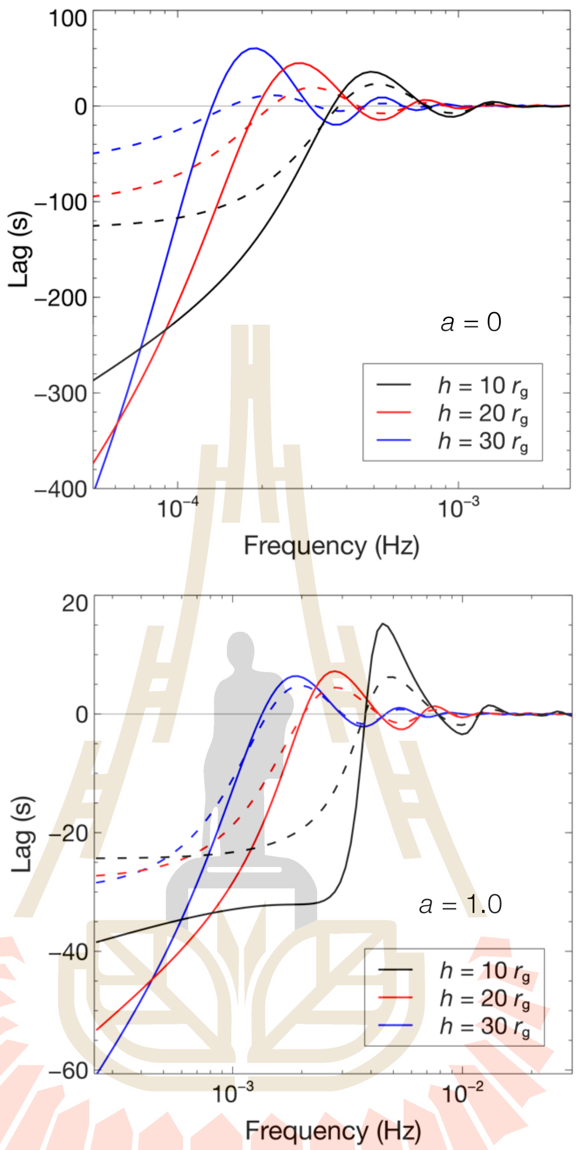

Figure 3.1 The comparison of simulated lag-frequency spectra using **`KYNxilrev`** (dashed lines) and **`KYNrefrev`** (solid lines) between the AGN with spin parameter, a = 0 (upper panel) and 1 (lower panel). In each panel, the coronal height was varied to be 10, 20 and 30 r_g shown in black, red, and blue, respectively. Other AGN parameters were fixed that i = 30°, Γ = 2.0 and L = 0.001 L_{Edd}. Figure adapted from Khanthasombat et al., 2024.

To sort the simulated lag amplitude (τ_{sim}) and frequency (ν_{sim}) that match τ_{obs} and ν_{obs}, the lag spectra are binned using the bin size comparable to those typically used in the timing analysis of the AGN such as 1H0707–495 and IRAS 13224–3809 (Caballero-García et al., 2018, 2020). Then, τ_{sim} is determined from the frequency bin that is before the phase wrapping occurs. The central frequency of that bin is used as a proxy for ν_{sim}. Then, for a given M_{BH}, we check for the consistency between the observed and the simulated lag values, by allowing ~ 20 and 2 per cent of the deviations between τ_{sim} and τ_{obs}, and between ν_{sim} and ν_{obs}, respectively. The effects of this allowed uncertainty are also investigated. All simulated spectra whereby phase wrapping occurs at frequencies below ν_{obs} are excluded. Only the samples that are consistent with the observed mass-scaling relation are included as the mock AGN samples for further analysis.

The fluctuations along the accretion disc that propagate inwards on longer timescales than those from the inner disc reflection can produce the positive hard lags at relatively low frequencies (Kotov, Churazov, and Gilfanov, 2001; Arevalo and Uttley, 2006). We note that De Marco et al. (2013) identified the value of the soft lag and the associating frequency from the amplitude and the frequency of the minimum point in the negative-lag profile, which is possible since the positive and negative lags can be clearly distinguished from the observed data. Here, we model only the negative reverberation lags so the minimum point as in De Marco et al. (2013) cannot be easily identified (i.e. we do not know the amount of the competing positive lags and the highest frequencies where they are possibly dominated). Instead, we choose to determine the value of the soft lag from the frequency bin just before the phase wrapping to ensure that the clean reverberation signature is probed. Nevertheless, for the accepted AGN data, the frequency bin where the lag is seen must also match the frequency bin reported by De Marco et al. (2013). This further ensures that our mocked data have both lag amplitude and the corresponding frequency following the mass-scaling law. An uncertainty due to the effect of the positive hard lags is also discussed in Appendix A2.

The flowchart illustrating the overall workflow of this work is presented in Figure 3.2. After the mock AGN samples that obey the mass-scaling law are obtained, the parameters derived from the `KYNxilrev` and `KYNrefrev` models are compared. While we perform 25,000 simulations of the lag frequency spectra, there are ~117 (115) of them produced from `KYNxilrev` (`KYNrefrev`) that fit in the lag-mass scaling relation and are accepted under our criteria. The correlations between the parameters implied from both models are then investigated. Finally, we allow the lag-mass scaling relation to deviate from the current trend and see its global effect on the parameters of the system.

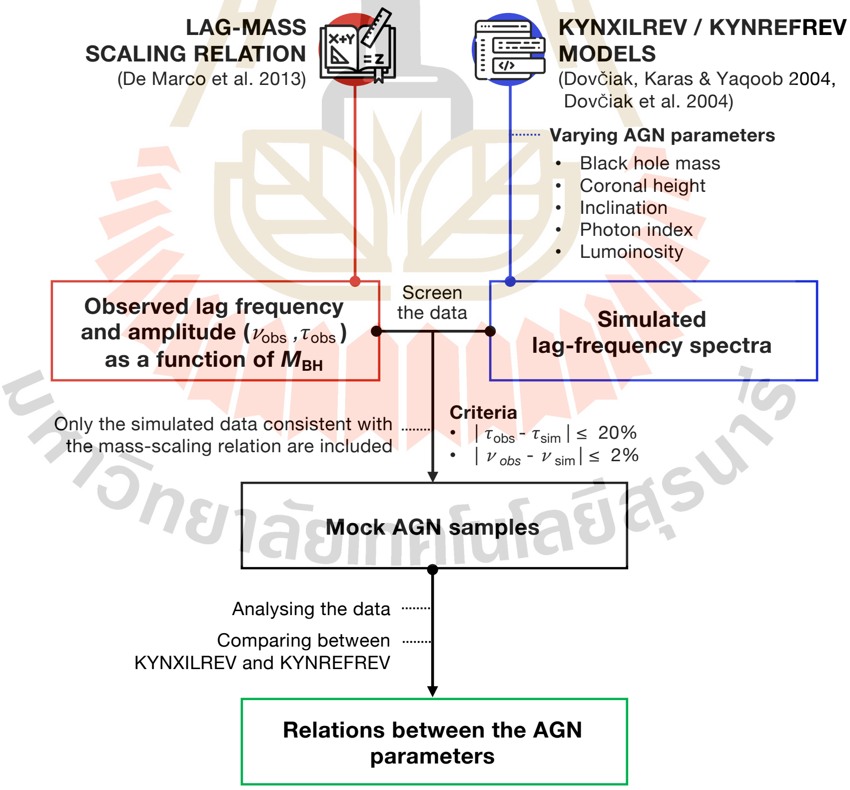

Figure 3.2 The flowchart representing the investigation process for this work. Figure from Khanthasombat et al., 2024.

CHAPTER IV

RESULTS

This following section is from the manuscript, titled “Parameter dependency on the public X-ray reverberation models **`KYNxilrev`** and **`KYNrefrev`**”. It was originally included there in section 4, the “Result” and “Lag-mass scaling relation and data simulation”. The manuscript is now accepted for publication in Monthly Notices of the Royal Astronomical Society (MNRAS) in 2024.

Once the mock AGN samples that match the mass-scaling law are gathered, the relations of their obtained parameters including time lag (τ), $M_{\rm BH}$, h, i, Γ, and L are analyzed. Figure 4.1 illustrates the relations between the observed lags and other parameters, comparing between what was derived by the **`KYNxilrev`** and **`KYNrefrev`** models. The moderate monotonic correlation between τ and h is significant ($p < 0.05$), with the Spearman’s rank correlation coefficient of r_s = 0.39 and 0.33 for **`KYNxilrev`** and **`KYNrefrev`**, respectively. However, the **`KYNxilrev`** model suggests more solutions towards lower lags and lower source height that can still follow the mass-scaling law. The lags are found to correlate with the luminosity only when using the **`KYNrefrev`** model, where r_s = 0.55. There is no correlation between the lags and inclination, and between the lags and photon index of the X-ray continuum from either **`KYNxilrev`** or **`KYNrefrev`** model.

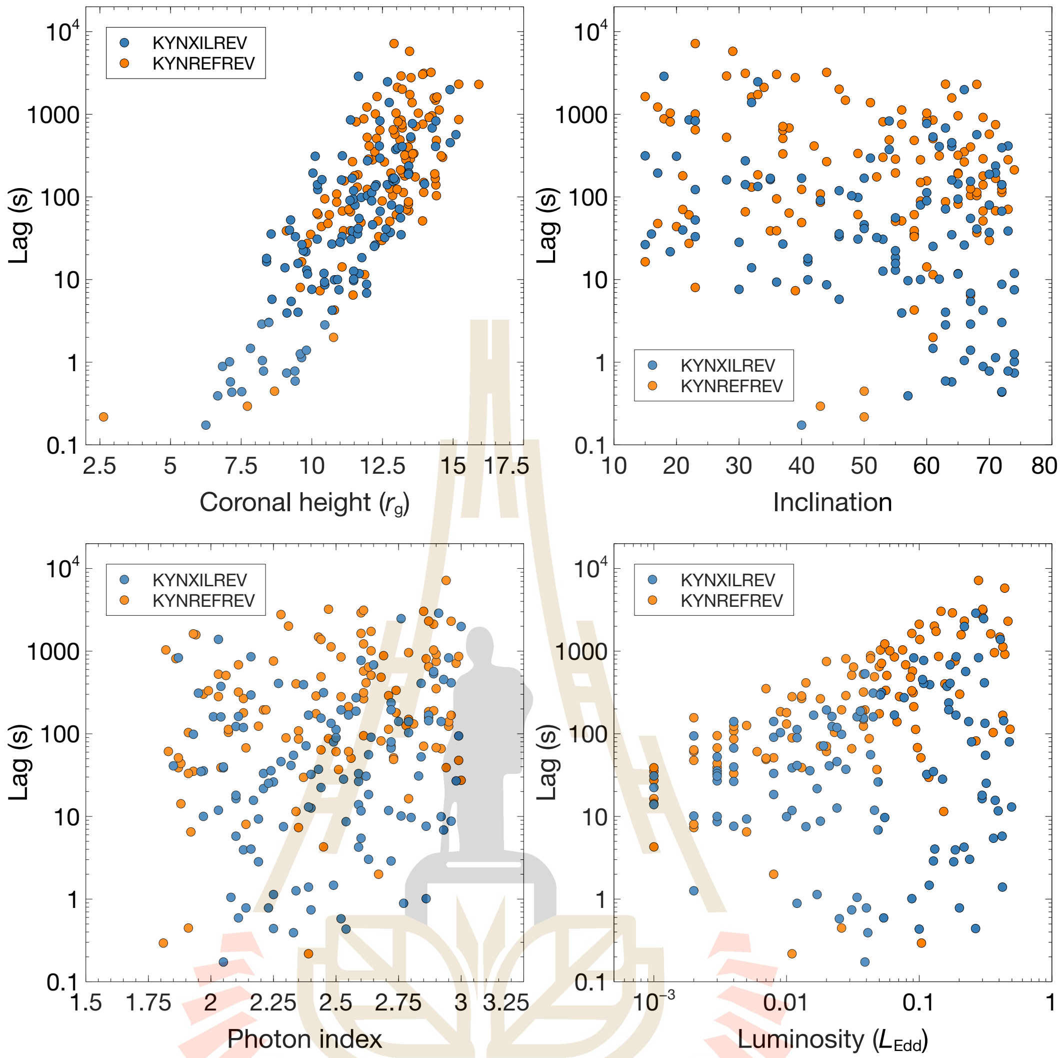

Figure 4.1 The relations between time lags and other parameters of the mock AGN samples that follow the lag-mass scaling law as obtained by `KYNxilrev` (blue) and `KYNrefrev` (orange). See text for more details. Figure from Khanthasombat et al., 2024.

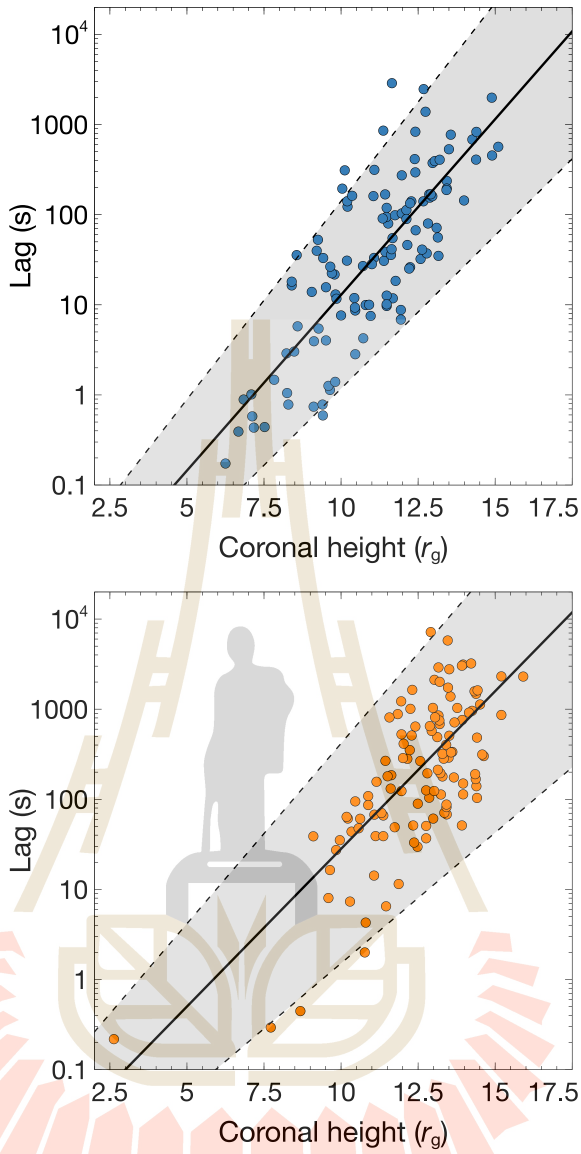

Figure 4.2 The best fit to the τ–h relation implied from **`KYNxilrev`** (upper panel) and **`KYNrefrev`** (lower panel). The 1–σ standard errors associated with the respective regression coefficients are overplotted on the data as the grey-shaded region between dashed lines. Figure from Khanthasombat et al., 2024.

The τ–h relation shown in Figure 4.1 suggests that, in addition to the black hole mass, the observed lags also depend on the height of the corona, which varies in all AGN. We then derive the τ–h relation by performing linear regression fitting to the data obtained from **`KYNxilrev`** and **`KYNrefrev`** models. While we perform 25,000 simulations of the lag frequency spectra, there are ~ 117 (115) of them produced from **KYNxilrev** (**KYNrefrev**) that fit in the lag-mass scaling relation and are accepted to create the plots, e.g., in Figure 4.1. The fitting results are presented in Figure 4.2. We find that the τ–h relation can be written in the form of

$$\log(|\tau|) = -2.79[\pm 0.32] - 0.39[\pm 0.03]\,h, \qquad [8]$$

and,

$$\log(|\tau|) = -2.05[\pm 0.39] - 0.35[\pm 0.03]\,h, \qquad [9]$$

for **KYNxilrev** and **KYNrefrev** models with corresponding R^2 = 0.63 and 0.53, respectively. Note that R^2 is the coefficient of determination that represents the variation from the true values of a dependent variable as predicted by the regression model (R^2 = 1 is a perfect fit). The uncertainty of each model coefficient is estimated from the 1–σ standard error calculated by taking the square root of the diagonal elements of the obtained covariance matrix.

Then, we investigate whether the lag-mass scaling relation prefers any specific value of the black hole spin. The spin parameters are varied to be a = 0, 0.5 and 1 for both models. Note that other parameters are uniformly varied within the range specified in Table 3.1, and only the samples that are consistent with the mass-scaling law are included in the analysis.

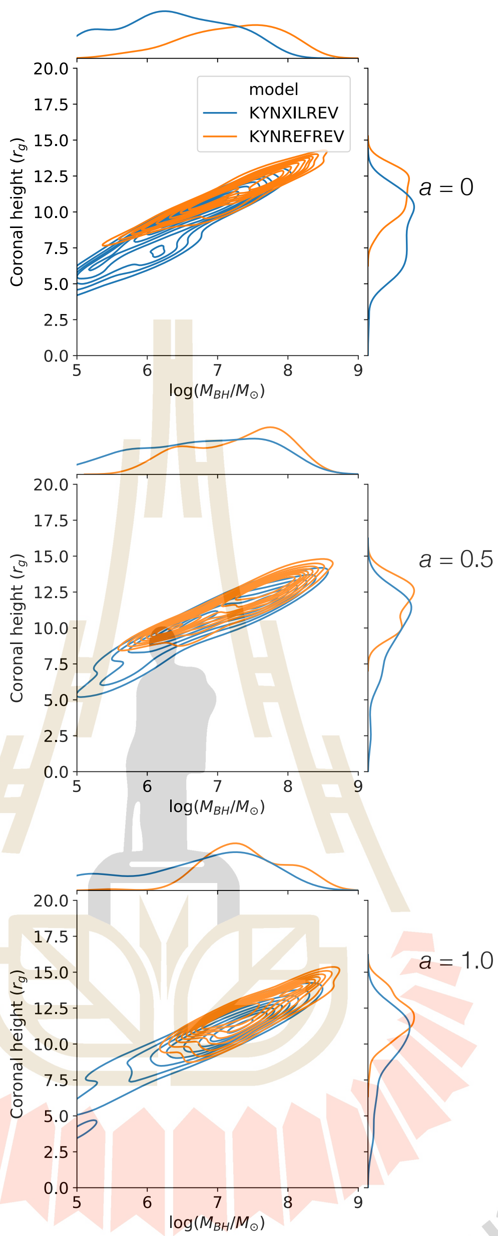

Figure 4.3 The relationship between the coronal height and the black hole mass of the mock AGN samples for different black hole spin of a = 0 (left panel), 0.5 (middle panel) and 1 (right panel). The results are generated and compared between the **`KYNxilrev`** (blue) and **`KYNrefrev`** (orange) models using the KDE. The curves outside the panels show the marginal distribution of the data for each parameter and model. Figure from Khanthasombat et al., 2024.

Figure 4.3 represents the h–M_{BH} distribution in the cases of low, medium, and high spin, derived from the layered kernel density estimate (KDE) in `seaborn` (Waskom, 2021). The KDE plot illustrates the smoothed-density distribution of the data using the Gaussian kernel with the contour lines to reveal the cluster and trend of the scattered data points. Interestingly, the solutions of low, medium, and high spin are all possible. Nevertheless, when $a = 0$ (upper panel), the `KYNxilrev` provides more samples at lower masses of $M_{BH} \lesssim 10^{6.5}\ M_{\odot}$, while the `KYNrefrev` model provides more samples at higher masses of $M_{BH} \gtrsim 10^{7.5}\ M_{\odot}$. This can lead to a bias due to the choice of the model used in determining the black hole mass and the coronal height in AGN that host a low-spin black hole. Even though the preferred solutions of h and M_{BH} for both models become more consistent in the cases of $a = 0.5$ and 1, the tendency that the `KYNxilrev` suggests the lower mass and lower source height is still noticeable. Despite this, both models strongly suggest the correlation between h and M_{BH}, regardless of the black hole spin.

The scatter plots for the simulated data showing the relation between h, M_{BH} and i when $a = 1$ are presented in Figure 4.4. Here, we also illustrate how the choice of the acceptable errors, $\Delta\tau_{err}$, affects the results. When $\Delta\tau_{err}$ decreases from within 20 to 10 per cent, the number of the solutions decreases which is expected since in doing this we accept only the mock samples that show more alignment with the observed scaling relation. By changing the threshold to accept the amplitude of the lag from 20 to 10 percent, the number of sets of parameters produced from `KYNxilrev` (`KYNrefrev`) that are accepted decreases from ~ 117 (115) to 47 (59). In any case, both `KYNxilrev` and `KYNrefrev` show a similar trend where the corona tends to be located at a higher gravitational height for a larger M_{BH}. Interestingly, this suggests that we can perhaps establish the h–M_{BH} scaling relation as what is done for the τ–M_{BH} relation. We then fit the h–M_{BH} data with a linear model. For `KYNxilrev` and `KYNrefrev` models, the best-fit h–M_{BH} relations are

$$h = -3.63[\pm1.04] + 2.20[\pm0.16] \log (M_{BH}/M_{\odot}), \quad [10]$$

and,

$$h = -2.44[\pm1.31] + 2.07[\pm0.18] \log (M_{BH}/M_{\odot}), \quad [11]$$

where the obtained R^2 is 0.64 and 0.54, respectively. However, the coronal height and the black hole mass are limited at high ends to be $h \lesssim 15\ r_g$ and $M_{BH} \lesssim 10^{8.5}\ M_{\odot}$. The models with higher values of the coronal height than ~ 15 r_g produce the lags which are too long and the phase-wrapping also occurs at too low frequencies that do not fit in the mass scaling relation. Note that we also investigate the case when the disc is truncated before the ISCO. For a variable inner-disc radius, the slope from the best fit to the h–M_{BH} relation can be shallower (see Appendix A).

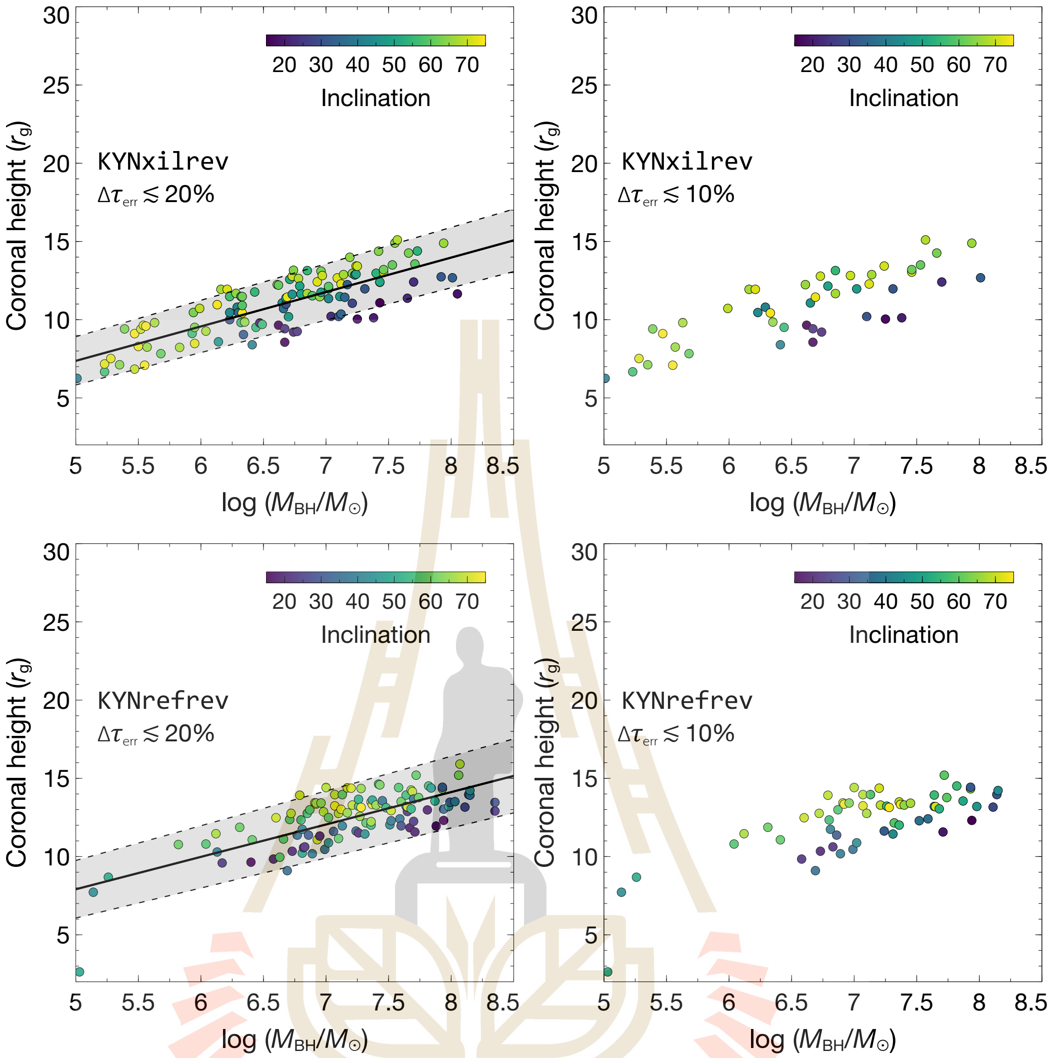

Figure 4.4 Obtained h–M_{BH} solutions from **`KYNxilrev`** (upper panels) and **`KYNrefrev`** (lower panels) models when the acceptable lag errors are limited to be within 20 (left panels) and 10 (right panels) per cent. The color indicates the value of the inclination angle (navy to yellow, i = 15°–75°). The solid line represents the best-fit linear model. The grey-shaded region between dashed lines shows the uncertainty estimated from the 1–σ standard errors of the respective model coefficients. Figure from Khanthasombat et al., 2024.

According to Figure 4.4, the inclination can be expected in the complete given range of 15°–75°, with small inclinations (20°–30°) commonly found in $M_{BH} \gtrsim 10^{6.5}\ M_\odot$.

Although the higher inclinations ($\geq 70°$) appear throughout the entire range of the mass for the **`KYNxilrev`**, they seem to be rarely found in **`KYNrefrev`** and only appear when $M_{BH} \sim 10^7\ M_{\odot}$. The trend of the mock samples remains almost the same even when the acceptable uncertainty, e.g. $\Delta\tau_{err}$, is changed and is not too small or too large. Therefore, from now on we evaluate and show the results by fixing the acceptable uncertainty at 20 per cent.

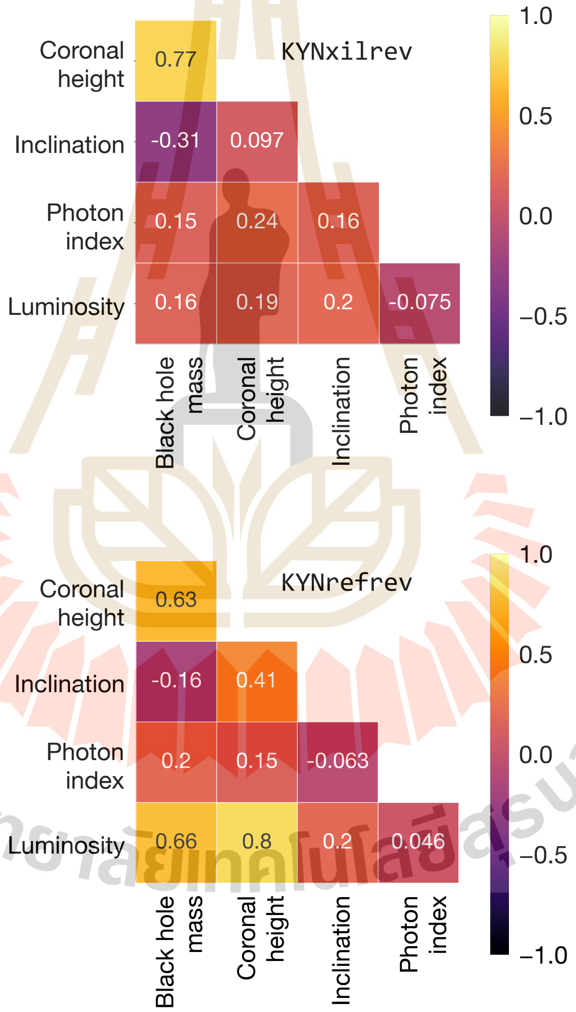

Figure 4.5 Spearman's rank correlation coefficient (r_s) between the obtained parameters constrained by the **`KYNxilrev`** (upper panel) and **`KYNrefrev`** (lower panel) models. Figure from Khanthasombat et al., 2024.

Overall correlations between each AGN parameter are presented in Figure 4.5. Both **`KYNxilrev`** and **`KYNrefrev`** reveal a strong monotonic correlation between h and M_{BH}, with the Spearman's rank correlation coefficient $r_s \sim 0.6$–0.8. The inclination is moderately correlated with the height ($r_s = 0.41$) for the **`KYNrefrev`** model, while this correlation is not observed when using **`KYNxilrev`**. Notably, the luminosity also shows a high correlation with the coronal height only in the case of **`KYNrefrev`** model ($r_s = 0.80$), while the **`KYNxilrev`** model does not reveal this correlation. An increasing trend of L with M_{BH} is also seen only in **`KYNrefrev`** data.

The distinct results of the L–h–M_{BH} relation obtained from both models are illustrated in Figure 4.6. The mock data from **`KYNxilrev`** appear to be more scattered with the additional data of $M_{\mathrm{BH}} \lesssim 10^6\ M_{\odot}$ compared to those from the **`KYNrefrev`**. These low mass data from the **`KYNxilrev`** model also correspond to relatively low source height and high luminosity, occupying the region in the parameter space where we find less solutions if using the **`KYNrefrev`** model. Comparing to Figure 4.4, these data are subjected to have high inclinations as well.

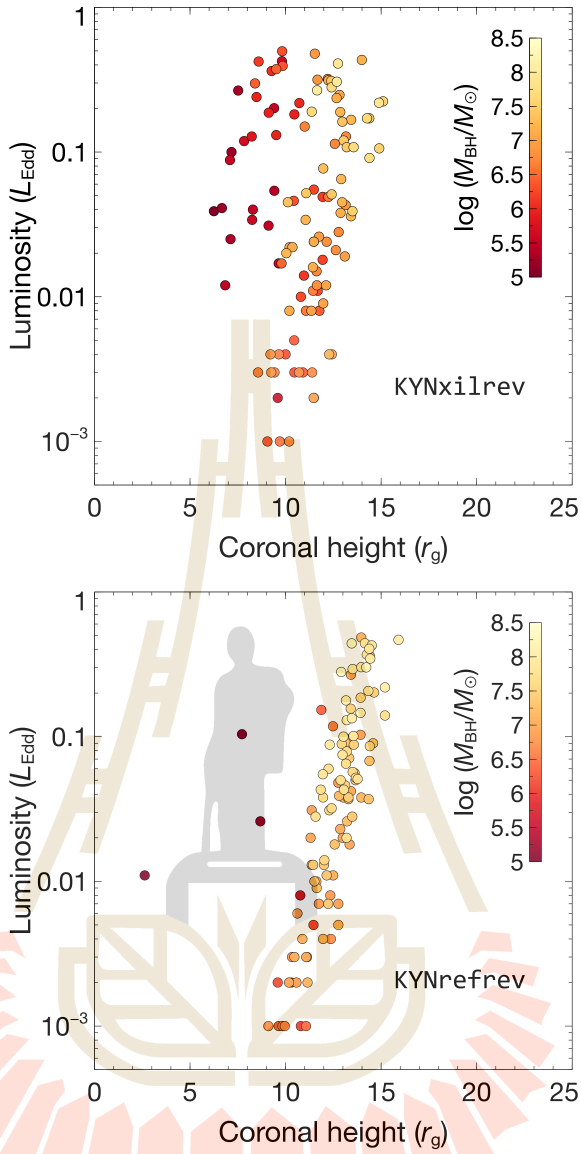

Figure 4.6 Comparison of the L–h relations derived by **`KYNxilrev`** (upper panel) and **`KYNrefrev`** (lower panel) models. Different colors indicate different MBH. Figure from Khanthasombat et al., 2024.

Furthermore, we investigate the effects when the slope of the observed lag-mass scaling relation (i.e. the coefficients on eqs. [4]–[5]) are deviated from the current trend. We adjust the slope of the τ–M_{BH} profile to be ±10 and ±20 per cent from the recent one and generate new mock AGN samples that follow the new τ–M_{BH} relation. The results are shown in Figure 4.7. It is clear that h and M_{BH} is still correlated in all cases. A larger number of higher-mass AGN possessing larger coronal height is expected if the coefficient of the lag-mass relation decreases. In other words, more solutions with higher h (up to ~ 20 r_g) can be found only when the data lies in the trend that has smaller coefficients than the observed one. By assuming the relation in the form of $h = x + y \log (M_{BH}/M_{\odot})$, we see that x vary approximately between -9 to -5 while y changes between 2.3 and 3. For a fixed mass, varying the slope of the lag-mass scaling law may represent the case when one looks at a particular AGN that exhibits different time lags as observed in different observations (see, e.g., Alston et al., 2020 in the case of IRAS 13224–3809 where the lags and the inferred coronal heights are varied across different observations).

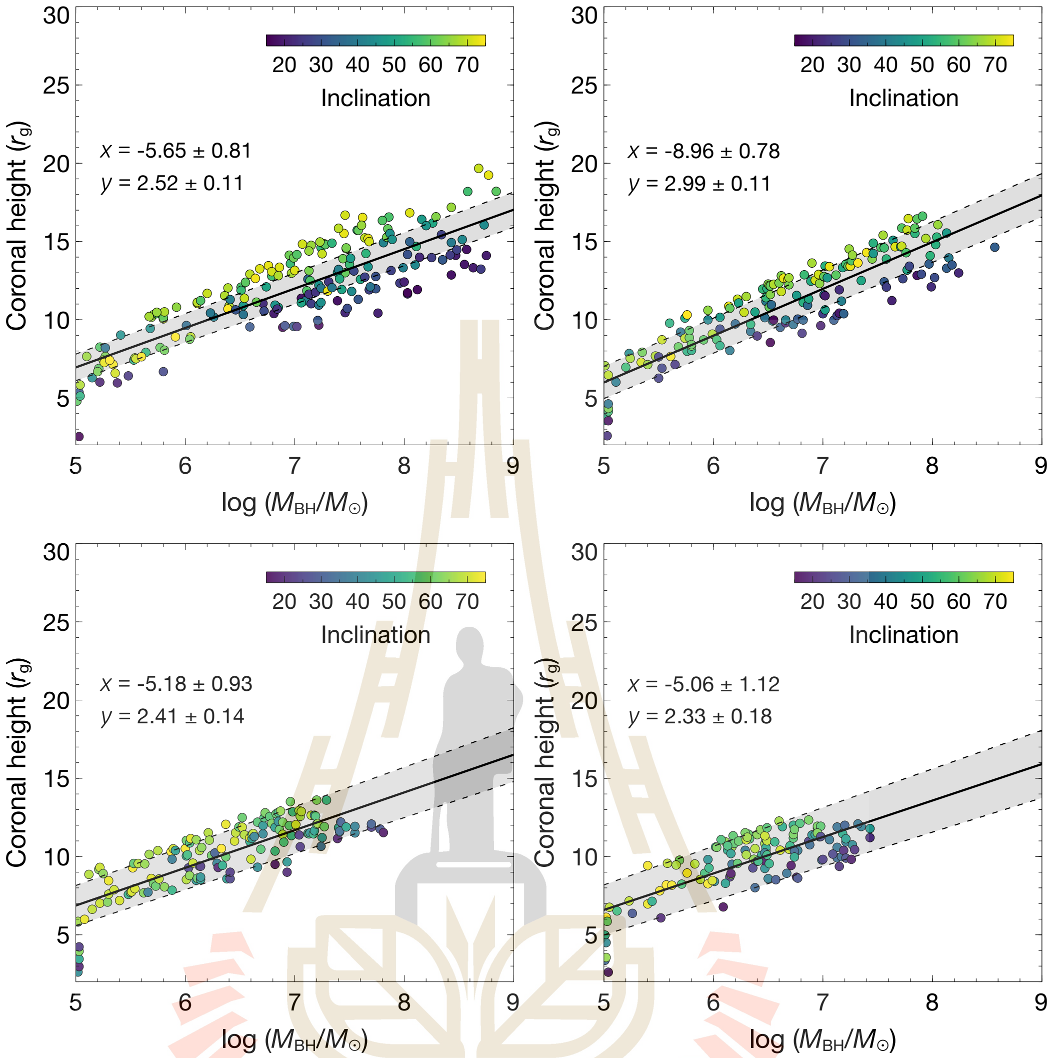

Figure 4.7 Obtained h–M_{BH} relations from the **`KYNxilrev`** model when the coefficient of the τ–M_{BH} scaling relation is changed to be −20, −10, +10 and +20 per cent from the current trend, from upper to lower panels. The best-fit linear model is in the form of $h = x + y \log(M_{BH}/M_{\odot})$, yielding a R^2 of 0.71, 0.80, 0.66 and 0.58, for the fits from upper to lower panels, respectively. Figure from Khanthasombat et al., 2024.

CHAPTER V

DISCUSSION AND CONCLUSION

This following section is from the manuscript, titled "Parameter dependency on the public X-ray reverberation models `KYNxilrev` and `KYNrefrev`". It was originally included there in section 5, the "Discussion and conclusion" and "Lag-mass scaling relation and data simulation". The manuscript is now accepted for publication in Monthly Notices of the Royal Astronomical Society (MNRAS) in 2024.

The X-ray reverberation lags in AGN were found to scale with the BH mass (De Marco et al., 2013; Kara et al., 2016; Hancock, Young, and Chainakun, 2022). By investigating Fe-L lags, De Marco et al. (2013) found that the lags roughly lie within the light crossing time for a distance of 6 r_g. Kara et al. (2016) analyzed the lags measured in the Fe-K band and found that the observed lags lie in the range of timescales corresponding to the light crossing distance of ~ 1–9 r_g. These previous studies suggest that the distances associated with X-ray reverberation are small, consistent with the inner disc reflection framework. However, the observed lag amplitudes are usually smaller than the intrinsic value due to the dilution effects caused by the cross-contamination of primary and reflection flux in the energy bands of interest (e.g. Kara et al., 2013; Wilkins and Fabian, 2013; Chainakun and Young, 2015). The true light travel distance then must be larger than those derived by converting the observed lags directly to the distance. Here, we follow the lag-mass scaling relation presented in De Marco et al. (2013) and generate mock AGN samples for testing the consistency between the `KYNxilrev` and `KYNrefrev` in explaining these data. Both models suggest that the observed lags are mass-dependent and can be triggered by a compact lamp-post source lying within $h \leq 15\ r_{\mathrm{g}}$.

The fact that the correlation coefficient between the lags and the mass is not intrinsically equal to 1 suggests that the lags must depend on other parameters as well. In addition to the black hole mass, it is likely that the observed lags also depend on the coronal height which is not the same in all AGN. The τ–h scaling relation is suggested either when using **`KYNrefrev`** or **`KYNxilrev`** model (Figure 4.2 and eqs. [8]–[9]). The slope of the τ–h fits from both models are comparable. Major differences between the **`KYNxilrev`** and **`KYNrefrev`** models are their underlying reflection spectra, **`xillver`** and **`reflionx`** respectively, where the reflection spectra employed by **`KYNxilrev`** were reported to exhibit a higher level of absorption particularly in the soft energy range of ~ 0.3–0.8 keV (García et al., 2013; Caballero-García et al., 2018). Despite this, both models still consistently infer the monotonic correlation between the coronal height in the gravitational units and the central mass. In fact, the height and the mass are correlated such that they can also be used as another independent scaling law (Figure 4.4 and eqs. [10]–[11]).

The results suggest that, by analyzing the Fe-L lags alone, the black hole spin cannot be well constrained. There is no preferred value of the black hole spin since the derived solutions from both models can match the mass-scaling law whether the black hole is non-, moderately-, or maximally-spinning. This is probably because the lag-frequency spectrum has a subtle change with the spin (Cackett et al., 2014). Even if this is the case, the **`KYNxilrev`** model seems to provide more solution towards lower h and lower MBH especially for a low-spin AGN.

Since the **`KYNxilrev`** model has more dilution, one would expect that this model requires longer intrinsic lags and higher coronal heights to explain the observed data. However, `KYNxilrev` allows smaller values of height compared to `KYNrefrev`. This is because, for a fixed coronal height, the reverberation lag from `KYNxilrev` is smaller than that from `KYNrefrev`, but their phase wrapping occurs at the same frequency (Figure 3.1). When the `KYNxilrev` model requires a higher source height to explain the lags, the phase-wrapping also shifts to lower frequencies than that from the `KYNrefrev` model, thus it no longer matches the mass scaling relation.

Alston et al. (2020) simultaneously fit the lag-frequency spectra in 16 XMM-Newton observations of IRAS 13224–3809 using the `KYNrefrev` model. While the variation of coronal height in IRAS 13224–3809 was found to be $h \sim 6$–$20\ r_g$, the majority of the obtained heights were found to be $h \leq 13\ r_g$. Note that the h–M_{BH} relation obtained when the slope of the lag-mass scaling law is varied can show how much the coronal height can change for a fixed mass. Given the IRAS 13224–3809 mass of $\log(M_{BH}/M_{\odot}) \sim 6.38$ (Alston et al., 2020), their upper limit of the height is roughly consistent with our possible heights at that particular mass. Caballero-García et al. (2020) investigated the combined spectral-timing data of IRAS 13224–3809 and found that, for the maximally spinning case, the source height could vary between ~ 3–$10\ r_g$. Recently, Mankatwit et al. (2023) utilizes a random forest regressor machine-learning model to investigate the X-ray reverberation lags due to the lamp-post corona in IRAS 13224–3809 and 1H 0707–495 using the response functions from the `KYNxilrev` model. Their constrained heights were also varied between 5–18 r_g. Following the current lag-mass scaling relation, it is rare that the AGN would occupy the lamp-post corona at a distance larger than $\sim 15\ r_g$. Otherwise, the coefficients of the mass scaling law need to deviate from the current trend by about 20 per cent (Figure 4.7).

De Marco et al. (2013) also investigated whether the lag timescales show some dependence on the source luminosity. They found a less significant correlation between the Fe-L lags and either the 2–10 keV or bolometric luminosity. Here, the significantly strong or even moderate correlations between the lags and the L cannot be observed. In fact, our results suggest that we should not expect to see the correlations between the lags and either Γ or i too (Figure 4.1). This means that L, Γ and i are not the key parameters that could place constraints on the lags and the disc-corona geometry in AGN. By using the Fe-K lags instead, Kara et al. (2016) found that the coronal height is correlated with the Eddington ratio, with the Spearman's rank correlation coefficient r_s = 0.61. Here, we found a strong correlation between the source height and the source luminosity (r_s = 0.80), but only when using the `KYNrefrev` model (Figure 4.6). This leads us to question if there really is a true correlation between the source geometry and luminosity, or if it is dependent on the choice of the reflection and reverberation models.

The extended study from Mallick et al. (2021) included more samples of low-mass AGNs ($M_{BH} < 3\times10^6\ M_\odot$) to the mass-scaling investigation. The equation of the lag-mass scaling is suggested to be comparable to those of De Marco et al., 2013), confirming that the soft lag amplitude in higher-mass AGN can be scaled with the mass to infer the lags in lower-mass AGN. Furthermore, they found that the corona extends at an average height of ~ 10 r_g on the symmetry axis. Our results suggest that the coronal height at ~ 10 r_g can potentially be found from low-mass to high-mass end of AGN (Figure 4.4) either using `KYNxilrev` or `KYNrefrev`. The deviation of the lag-mass equations comparing between De Marco et al. (2013) and Mallick et al. (2021) should be within the ±20 per cent of the lag variations allowed in this work (see Figure 9), so our results should still be representative either for the samples of low- or high-mass AGN in previous literature.

Our obtained h–M_{BH} relation suggests that the corona in lower-mass AGN tends to be more compact than the corona in higher-mass AGN. Although timing analysis under the lamp-post assumption successfully determines the coronal geometry

(Caballero-García et al., 2018), it may prefer higher source heights compared to the method using the time-averaged spectra (Alston et al., 2020; Chainakun et al., 2022; Jiang et al., 2022). The real corona should extend, and different parts may vary differently. The extended corona was suggested in many studies to have an ability to influence the time-lag spectra that can explain the data (Wilkins et al., 2016; Chainakun and Young, 2017; Hancock, Young, and Chainakun, 2023; Lucchini et al., 2023). In this case, the same corona geometry can produce different reverberation lag amplitudes by varying its properties such as the optical depth (Chainakun et al., 2019) and the propagating fluctuations inside the corona (Wilkins et al., 2016), or by assuming different disc geometry (Taylor and Reynolds 2018; Kawamura, Done, and Takahashi, 2023). Adjusting these are not possible for the current `KYNxilrev` and `KYNrefrev` models.

Furthermore, Wilkins et al. (2020) developed a modified `xillver` model referred to as `XILLVER`RR to study the returning radiation that can cause extra reverberation delays due to secondary or even higher order reflections. The results show that, for the black hole with the spin a = 0.998 and the corona at h = 5 r_g, almost 40 per cent of the photons will experience the returning process. The returning fraction will decrease as the X-ray source height increases, with the crucial point at h = 10 r_g where the photons are more likely to travel directly to the observer. Both `KYNxilrev` and `KYNrefrev` do not take into account the extra time delays due to the returning radiation. This can lead to an uncertainty in the measurement of the coronal height especially at $h \leq 5$ r_g where the returning radiation should play an important role. As for that, the obtained source height at $h \leq 5$ r_g could, in fact, be smaller if we consider the effect of the returning radiation. However, this effect will similarly apply to both models, by mainly adding extra light-travel time so it should not change the comparative results between both models. Furthermore, the effects of non-uniform orbiting clouds that introduce the covering fraction (Hancock, Young, and Chainakun, 2022) and extra dilutions that may occur due to environmental absorption (Parker et al., 2021) are not taken into account in calculating the lags. A recent study by Jaiswal et al. (2023) suggested that the effect of the scattering of the disc emission by the broad line region on the time delay is quite similar to the effect of increasing the X-ray source height. Again, the non-quantitative comparison of **KYNxilrev** and **KYNrefrev** should still be valid since all these effects will similarly apply over both models.

In conclusion, the maximum coronal height inferred by **KYNrefrev** and **KYNxilrev** models that assumes a lamp-post model for a distant observer is likely limited at $h \leq 15$–$20\ r_g$. This should be true for any newly-discovered AGN if their lags and mass follows the current scaling-relation trend. The average source height at $h \sim 10\ r_g$ can be found either in low or high mass AGN. Our results reveal that there is a high chance that the lower-mass AGN has a more compact corona located at a lower height on the symmetry axis. As for that, the h–M_{BH} scaling relation may be valid whether the coronal height is implied using **KYNrefrev** or **KYNxilrev** model. However, the differences of both models in explaining the X-ray timing data are clearly seen. There is an inconsistency that the **KYNxilrev** suggests a greater number of possible solutions with low MBH and low h than the **KYNrefrev**, especially for the low spinning black hole. Last but not least, the **KYNrefrev** models suggest a moderate monotonic correlation between the luminosity and the coronal height while the **KYNxilrev** does not. Therefore, when analysing a large number of data or observations, the derived parameter correlations may be model dependent.

REFERENCES

REFERENCES

Alston, W. N., Fabian, A. C., Kara, E., Parker, M. L., Dovčiak, M., Pinto, C., Jiang, J., Middleton, M. J., Miniutti, G., Walton, D. J., Wilkins, D. R., Buisson, D. J., Caballero-García, M. D., Cackett, E. M., De Marco, B., Gallo, L. C., Lohfink, A. M., Reynolds, C. S., Uttley, P., … Zogbhi, A. (2020). A dynamic black hole Corona in an active galaxy through X-ray reverberation mapping. *Nature Astronomy*, *4*(6), 597–602. https://doi.org/10.1038/s41550-019-1002-x

Arevalo, P., and Uttley, P. (2006). Investigating a fluctuating-accretion model for the spectral-timing properties of accreting Black Hole Systems. *Monthly Notices of the Royal Astronomical Society*, *367*(2), 801–814. https://doi.org/10.1111/j.1365-2966.2006.09989.x

Bambi, C., Brenneman, L. W., Dauser, T., García, J. A., Grinberg, V., Ingram, A., Jiang, J., Liu, H., Lohfink, A. M., Marinucci, A., Mastroserio, G., Middei, R., Nampalliwar, S., Niedzwiecki, A., Steiner, J. F., Tripathi, A., and Zdziarski, A. A. (2021). Towards precision measurements of accreting black holes using X-ray reflection spectroscopy. *Space Science Reviews*, *217*(5). https://doi.org/10.1007/s11214-021-00841-8

Caballero-García, M. D., Papadakis, I. E., Dovčiak, M., Bursa, M., Epitropakis, A., Karas, V., and Svoboda, J. (2018). Testing the X-ray reverberation model KYNREFREV in a sample of Seyfert 1 active galactic nuclei. *Monthly Notices of the Royal Astronomical Society*. https://doi.org/10.1093/mnras/sty1990

Caballero-García, M. D., Papadakis, I. E., Dovčiak, M., Bursa, M., Svoboda, J., and Karas, V. (2020). A combined timing/spectral study of IRAS 13224-3809 using XMM–

Newton Data. *Monthly Notices of the Royal Astronomical Society*, *498*(3), 3184–3192. https://doi.org/10.1093/mnras/staa2554

Cackett, E. M., Zoghbi, A., Reynolds, C., Fabian, A. C., Kara, E., Uttley, P., and Wilkins, D. R. (2014). Modelling the broad Fe Kα reverberation in the AGN NGC 4151. *Monthly Notices of the Royal Astronomical Society*, *438*(4), 2980–2994. https://doi.org/10.1093/mnras/stt2424

Cackett, Edward M., Bentz, M. C., and Kara, E. (2021). Reverberation mapping of active galactic nuclei: From X-ray corona to dusty torus. *iScience*, *24*(6), 102557. https://doi.org/10.1016/j.isci.2021.102557

Chainakun, P, Nakhonthong, N., Luangtip, W., and Young, A. J. (2023). Revealing the intrinsic X-ray reverberation lags in IRAS 13224–3809 through the Granger Causality Test. Monthly Notices of the Royal Astronomical Society, 523(1), 111–122. https://doi.org/10.1093/mnras/stad1416

Chainakun, P, Watcharangkool, A., Young, A. J., and Hancock, S. (2019). X-ray time lags in AGN: Inverse-compton scattering and spherical Corona Model. *Monthly Notices of the Royal Astronomical Society*, *487*(1), 667–680. https://doi.org/10.1093/mnras/stz1319

Chainakun, P., and Young, A. J. (2015). Simultaneous spectral and reverberation modelling of relativistic reflection in MRK 335. *Monthly Notices of the Royal Astronomical Society*, *452*(1), 333–342. https://doi.org/10.1093/mnras/stv1333

Chainakun, P., and Young, A. J. (2017). Investigating the X-ray time lags in PG 1244+026 using an extended Corona model. *Monthly Notices of the Royal Astronomical Society*, *465*(4), 3965–3976. https://doi.org/10.1093/mnras/stw2964

Chainakun, P., Luangtip, W., Jiang, J., and Young, A. J. (2022). Mapping the X-ray corona evolution of IRAS 13224-3809 with the power spectral density. *The Astrophysical Journal*, *934*(2), 166. https://doi.org/10.3847/1538-4357/ac7d55

Dauser, T., García, J., Wilms, J., Böck, M., Brenneman, L. W., Falanga, M., Fukumura, K., and Reynolds, C. S. (2013). Irradiation of an accretion disc by a jet: General properties and implications for spin measurements of Black Holes. *Monthly Notices of the Royal Astronomical Society*, *430*(3), 1694–1708. https://doi.org/10.1093/mnras/sts710.

De Marco, B., Ponti, G., Cappi, M., Dadina, M., Uttley, P., Cackett, E. M., Fabian, A. C., and Miniutti, G. (2013). Discovery of a relation between black hole mass and soft X-ray time lags in active galactic nuclei. *Monthly Notices of the Royal Astronomical Society*, *431*(3), 2441–2452. https://doi.org/10.1093/mnras/stt339.

Dove, J. B., Wilms, J., and Begelman, M. C. (1997). Self-consistent thermal accretion disk corona models for compact objects. I. Properties of the Corona and the spectrum of escaping radiation. *The Astrophysical Journal*, *487*(2), 747–758. https://doi.org/10.1086/304632

Dovčiak, M., Karas, V., Martocchia, A., Matt, G., and Yaqoob, T. (2004). An XSPEC model to explore spectral features from black-hole sources. In Proceedings of RAGtime 4/5 Workshops on Black Holes and Neutron Stars, 33.

Dovčiak, M., Karas, V., and Yaqoob, T. (2004). An extended scheme for Fitting x-ray data with accretion disk spectra in the Strong Gravity Regime. *The Astrophysical Journal Supplement Series*, *153*(1), 205–221. https://doi.org/10.1086/421115.

Emmanoulopoulos, D., McHardy, I. M., and Papadakis, I. E. (2011). Negative X-ray reverberation time delays from MCG-6-30-15 and MRK 766. *Monthly Notices of the Royal Astronomical Society: Letters, 416(1).* https://doi.org/10.1111/j.1745-3933.2011.01106.x

Epitropakis, A., Papadakis, I. E., Dovčiak, M., Pecháček, T., Emmanoulopoulos, D., Karas, V., and McHardy, I. M. (2016). Theoretical modelling of the AGN Iron Line vs. Continuum Time-lags in the lamp-post geometry. *Astronomy and Astrophysics*, *594*. https://doi.org/10.1051/0004-6361/201527748.

Fabian, A. C., Celotti, A., Pooley, G., Iwasawa, K., Brandt, W. N., McMahon, R. G., and Hoenig, M. D. (1999). Variability of the extreme z = 4.72 blazar, GB 1428+4217. *Monthly Notices of the Royal Astronomical Society*, *308*(1). https://doi.org/10.1046/j.1365-8711.1999.02910.x.

Fabian, A. C., Zoghbi, A., Ross, R. R., Uttley, P., Gallo, L. C., Brandt, W. N., Blustin, A. J., Boller, T., Caballero-García, M. D., Larsson, J., Miller, J. M., Miniutti, G., Ponti, G., Reis, R. C., Reynolds, C. S., Tanaka, Y., and Young, A. J. (2009). Broad line emission from Iron K- and L-shell transitions in the active galaxy 1H 0707-495. *Nature*, *459*(7246), 540–542. https://doi.org/10.1038/nature08007.

Fabian, A. C., Iwasawa, K., Reynolds, C. S., and Young, A. J. (2000). Broad iron lines in active galactic nuclei. *Publications of the Astronomical Society of the Pacific*, *112*(775), 1145–1161. https://doi.org/10.1086/316610.

García, J., Dauser, T., Reynolds, C. S., Kallman, T. R., McClintock, J. E., Wilms, J., and Eikmann, W. (2013). X-ray reflected spectra from accretion disk models. III. A complete grid of ionized reflection calculations. *The Astrophysical Journal*, *768*(2), 146. https://doi.org/10.1088/0004-637x/768/2/146.

García, J., and Kallman, T. R. (2010). X-ray reflected spectra from accretion disk models. I. Constant Density Atmospheres. *The Astrophysical Journal*, *718*(2), 695–706. https://doi.org/10.1088/0004-637x/718/2/695.

García, J., Kallman, T. R., Witthoeft, M., Behar, E., Mendoza, C., Palmeri, P., Quinet, P., Bautista, M. A., and Klapisch, M. (2009). Nitrogen K-shell photoabsorption. *The Astrophysical Journal Supplement Series*, *185*(2), 477–485. https://doi.org/10.1088/0067-0049/185/2/477

García, J., Kallman, T. R., and Mushotzky, R. F. (2011). X-ray reflected spectra from accretion disk models. II. diagnostic tools for X-ray observations. *The Astrophysical Journal*, *731*(2), 131. https://doi.org/10.1088/0004-637x/731/2/131.

García, J., Mendoza, C., Bautista, M. A., Gorczyca, T. W., Kallman, T. R., and Palmeri, P. (2005). K-shell photoabsorption of oxygen ions. *The Astrophysical Journal Supplement Series*, *158*(1), 68–79. https://doi.org/10.1086/428712

George, I. M., and Fabian, A. C. (1991). X-ray reflection from cold matter in active galactic nuclei and X-ray binaries. *Monthly Notices of the Royal Astronomical Society*, *249*(2), 352–367. https://doi.org/10.1093/mnras/249.2.352

Grevesse, N., and Sauval, A. J. (1998). Standard Solar Composition. *Space Science Reviews*, *85*(1/2), 161–174. https://doi.org/10.1023/a:1005161325181

Hancock, S., Young, A. J., and Chainakun, P. (2022). X-ray timing and spectral analysis of reverberating active galactic nuclei. *Monthly Notices of the Royal Astronomical Society*, *514*(4), 5403–5421. https://doi.org/10.1093/mnras/stac1653

Hancock, S., Young, A. J., and Chainakun, P. (2023). Extended Corona models of X-ray reverberation in the AGN 1H 0707−495 and IRAS 13224−3809. *Monthly Notices of the Royal Astronomical Society*, *520*(1), 180–192. https://doi.org/10.1093/mnras/stad144

Jaiswal, V. K., Prince, R., Panda, S., and Czerny, B. (2023). Modeling time delays from two reprocessors in active galactic nuclei. *Astronomy andamp; Astrophysics*, *670*. https://doi.org/10.1051/0004-6361/202244352

Jiang, J., Dauser, T., Fabian, A. C., Alston, W. N., Gallo, L. C., Parker, M. L., and Reynolds, C. S. (2022). XMM–newton observations of the narrow-line Seyfert 1 galaxy IRAS 13224−3809: X-ray spectral analysis II. *Monthly Notices of the Royal Astronomical Society*, *514*(1), 1107–1121. https://doi.org/10.1093/mnras/stac1144

Kallman, T. R., Palmeri, P., Bautista, M. A., Mendoza, C., and Krolik, J. H. (2004). Photoionization modeling and the K lines of iron. *The Astrophysical Journal Supplement Series*, *155*(2), 675–701. https://doi.org/10.1086/424039

Kallman, T., and Bautista, M. (2001). Photoionization and high-density gas. *The Astrophysical Journal Supplement Series*, *133*(1), 221–253. https://doi.org/10.1086/319184

Kara, E., Alston, W. N., Fabian, A. C., Cackett, E. M., Uttley, P., Reynolds, C. S., and Zoghbi, A. (2016). A global look at X-ray time lags in Seyfert galaxies. *Monthly Notices of the Royal Astronomical Society*, *462*(1), 511–531. https://doi.org/10.1093/mnras/stw1695

Kara, E., Cackett, E. M., Fabian, A. C., Reynolds, C., and Uttley, P. (2013). The Curious Time Lags of PG 1244+026: Discovery of the iron K reverberation lag. *Monthly Notices of the Royal Astronomical Society: Letters*, *439*(1). https://doi.org/10.1093/mnrasl/slt173

Kawamura, T., Done, C., and Takahashi, T. (2023). The origin of Long Soft Lags and the nature of the hard-intermediate state in black hole binaries. *Monthly Notices of the Royal Astronomical Society*, *525*(1), 1280–1287. https://doi.org/10.1093/mnras/stad2338

Khanthasombat, K., Chainakun, P., and Young, A. J. (2024). Parameter dependency on the public X-ray reverberation models kynxilrev and kynrefrev. *Monthly Notices of the Royal Astronomical Society, 528(2),* 3130–3140. https://doi.org/10.1093/mnras/stae173

Kotov, O., Churazov, E., and Gilfanov, M. (2001). On the X-ray time-lags in the Black Hole candidates. *Monthly Notices of the Royal Astronomical Society*, *327*(3), 799–807. https://doi.org/10.1046/j.1365-8711.2001.04769.x

Lucchini, M., Mastroserio, G., Wang, J., Kara, E., Ingram, A., García, J., Dauser, T., van der Klis, M., König, O., Lewin, C., Nathan, E., and Panagiotou, C. (2023). Investigating the impact of vertically extended coronae on X-ray reverberation mapping. *The Astrophysical Journal*, *951*(1), 19. https://doi.org/10.3847/1538-4357/acd24f

Mallick, L., Wilkins, D. R., Alston, W. N., Markowitz, A., De Marco, B., Parker, M. L., Lohfink, A. M., and Stalin, C. S. (2021). Discovery of soft and hard X-ray time lags in low-mass agns. *Monthly Notices of the Royal Astronomical Society*, *503*(3), 3775–3783. https://doi.org/10.1093/mnras/stab627

Mankatwit, N., Chainakun, P., Luangtip, W., and Young, A. J. (2023). Coronal height constraint in IRAS 13224–3809 and 1H 0707–495 by the Random Forest Regressor. *Monthly Notices of the Royal Astronomical Society*, *523*(3), 4080–4088. https://doi.org/10.1093/mnras/stad1706

Morrison, R., and McCammon, D. (1983). Interstellar Photoelectric Absorption Cross Sections, 0.03-10 Kev. *The Astrophysical Journal*, *270*, 119. https://doi.org/10.1086/161102

Novikov, I. D., and Thorne, K. S. (1973). Astrophysics of black holes. *Black Holes (Les Astres Occlus)*, *343*.

Nowak, M. A., Vaughan, B. A., Wilms, J., Dove, J. B., and Begelman, M. C. (1999). rossi x-ray timing explorer observation of Cygnus X-1. II. timing analysis. *The Astrophysical Journal*, *510*(2), 874–891. https://doi.org/10.1086/306610

Palma, N. I., Böttcher, M., de la Calle, I., Agudo, I., Aller, M., Aller, H., Bach, U., Benítez, E., Buemi, C. S., Escande, L., Gómez, J. L., Gurwell, M. A., Heidt, J., Hiriart, D., Jorstad, S. G., Joshi, M., Lähteenmäki, A., Larionov, V. M., Leto, P., ... Wylezalek, D. (2011). Multiwavelength observations of the gamma-ray blazar PKS 0528+134 in quiescence. The Astrophysical Journal, *735*(1), 60. https://doi.org/10.1088/0004-637x/735/1/60

Parker, M. L., Alston, W. N., Härer, L., Igo, Z., Joyce, A., Buisson, D. J., Chainakun, P., Fabian, A. C., Jiang, J., Kosec, P., Matzeu, G. A., Pinto, C., Xu, Y., and Zaidouni, F. (2021). The nature of the extreme X-ray variability in the NLS1 1H 0707-495. *Monthly Notices of the Royal Astronomical Society*, *508*(2), 1798–1816. https://doi.org/10.1093/mnras/stab2434

Reynolds, C. S., Young, A. J., Begelman, M. C., and Fabian, A. C. (1999). X-Ray iron line reverberation from black hole accretion disks. *The Astrophysical Journal*, *514*(1), 164–179. https://doi.org/10.1086/306913.

Ross, R. R., and Fabian, A. C. (2005). A comprehensive range of X-ray ionized-reflection models. *Monthly Notices of the Royal Astronomical Society*, *358*(1), 211–216. https://doi.org/10.1111/j.1365-2966.2005.08797.x

Ross, R. R., Fabian, A. C., and Young, A. J. (1999). X-ray reflection spectra from ionized slabs. *Monthly Notices of the Royal Astronomical Society*, *306*(2), 461–466. https://doi.org/10.1046/j.1365-8711.1999.02528.x

Taylor, C., and Reynolds, C. S. (2018). X-ray reverberation from black hole accretion disks with realistic geometric thickness. *The Astrophysical Journal*, *868*(2), 109. https://doi.org/10.3847/1538-4357/aae9f2

Uttley, P., Cackett, E. M., Fabian, A. C., Kara, E., and Wilkins, D. R. (2014). X-ray reverberation around accreting Black Holes. *The Astronomy and Astrophysics Review*, *22*(1). https://doi.org/10.1007/s00159-014-0072-0

Waskom, M. (2021). Seaborn: Statistical data visualization. *Journal of Open Source Software*, *6*(60), 3021. https://doi.org/10.21105/joss.03021

Wilkins, D. R., and Fabian, A. C. (2013). The origin of the lag spectra observed in AGN: Reverberation and the propagation of X-ray source fluctuations. *Monthly Notices of the Royal Astronomical Society*, *430*(1), 247–258. https://doi.org/10.1093/mnras/sts591

Wilkins, D. R., Cackett, E. M., Fabian, A. C., and Reynolds, C. S. (2016). Towards modelling X-ray reverberation in AGN: Piecing together the extended Corona. *Monthly Notices of the Royal Astronomical Society*, *458*(1), 200–225. https://doi.org/10.1093/mnras/stw276

Wilkins, D. R., García, J. A., Dauser, T., and Fabian, A. C. (2020). Returning radiation in strong gravity around black holes: Reverberation from the accretion disc. *Monthly Notices of the Royal Astronomical Society*, *498*(3), 3302–3319. https://doi.org/10.1093/mnras/staa2566

APPENDICES

APPENDIX A

VARIABLE INNER-DISC RADIUS

This following section is from the manuscript, titled “Parameter dependency on the public X-ray reverberation models **`KYNxilrev`** and **`KYNrefrev`**”. It was originally included there in appendix A, the “Variable inner-disc radius” and “Lag-mass scaling relation and data simulation”. The manuscript is now accepted for publication in Monthly Notices of the Royal Astronomical Society (MNRAS), in press.

We further investigate the case of a variable inner-disc radius. We fix a = 1, i = 45°, Γ = 2.0 and L/L_{Edd} = 0.1 while randomly vary the truncation radius of the disc. Other parameters including MBH and h are allowed to vary in the range given in Table 3.1. The result is shown in Figure A1. While the lag is driven mostly by the distance between the corona and the disc, a larger truncation radius results in a larger distance for the coronal photons to travel to the inner edge of the disc, hence producing a longer lag. Therefore, if the disc is allowed to be truncated, there is a chance to get lower values of the height for a given mass, as can be seen in a clear separation of color in the h–M_{BH} relation. There is only a minority of the data that show higher coronal heights for a truncated disc compared to when the disc is fixed to ISCO. This inconsistency should arise due to the fact that we allow some threshold levels of the lag amplitude. However, the accreting supermassive black holes in AGN are mostly rapidly spinning and we do not expect the AGN disc to be significantly truncated since the broad emission lines are often observed Reynolds (2021).

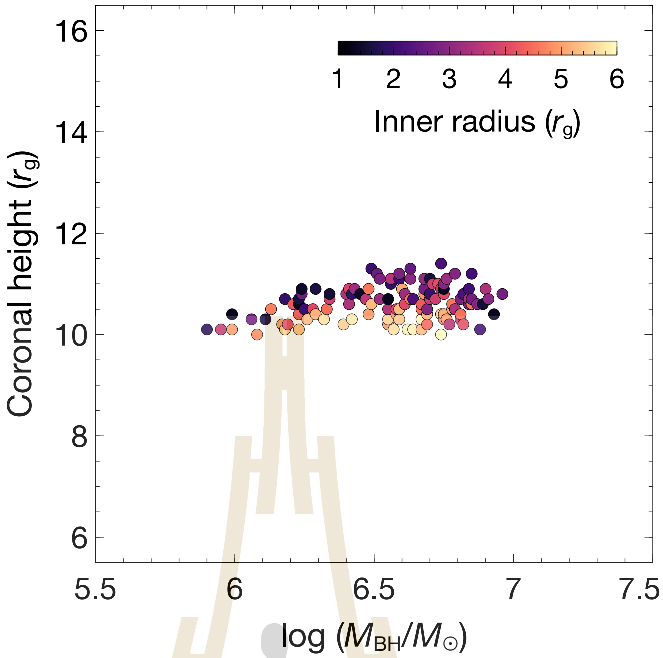

Figure A1 The h–M_{BH} relation from **`KYNxilrev`** when a = 1 and the inner-disc radius is allowed to vary randomly between ISCO and 6 r_g. We fix i = 45°, Γ = 2.0 and L/L_{Edd} = 0.1 in this illustration. For a variable inner radius, the model provides more possible solutions with lower source heights for a given mass. Figure from Khanthasombat et al., 2024.

APPENDIX B

SOURCES OF UNCERTAINTY

This following section is from the manuscript, titled “Parameter dependency on the public X-ray reverberation models **`KYNxilrev`** and **`KYNrefrev`**”. It was originally included there in appendix A, the “Variable inner-disc radius” and “Lag-mass scaling relation and data simulation”. The manuscript is now accepted for publication in Monthly Notices of the Royal Astronomical Society (MNRAS), in press.

We note an effect of the positive hard lags due to the inward propagation of fluctuations in the disc (Ar´evalo and Uttley, 2006) that may contribute to the uncertainty in our results. The observed reverberation lags further away from the phase wrapping towards lower frequencies will be likely more affected by the propagating-fluctuation lags that operate on relatively long timescales. In Figure A2, we show how this competing process can affect the reverberation lags at frequencies where we expect to see the reverberation lags. A full modelling of the disc-propagating fluctuations could be an option but it may lead to a significantly larger set of parameters. In Figure A2, the amplitude and frequency of the reverberation lag at the minimum point move closer to the phase wrapping frequency if the disc propagating-fluctuation signals become stronger. Also, if the coronal height increases, the phase wrapping point will move towards lower frequencies. The reason why large distances (e.g. $h \gtrsim 20\ r_{\rm g}$) between the lamp-post source and the disc do not explain the observations is probably because their phase wrapping frequencies are too low. Unless the true positive lags are known, there is always uncertainty in determining the exact frequency and amplitude of the minimum point in the negative-lag profiles.

Nevertheless, these uncertainties may be compensated more or less by 1) allowing some threshold levels of the lag amplitude and 2) investigating the cases when the mass scaling relation deviates from the current observed trend (Figure 4.7). Therefore, the results here should still be reliable and representative of the overall parameter relations.

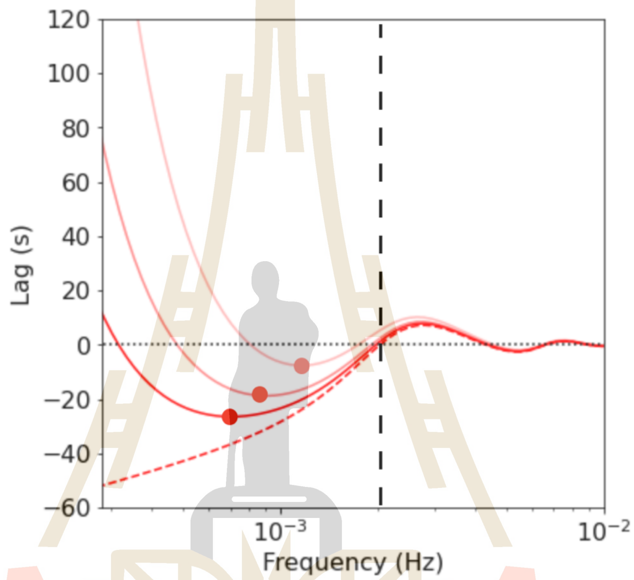

Figure A2 Simulated lag-frequency spectra from **KYNrefrev** (red dashed line) where the vertical dashed line identifies the phase-wrapping frequency. Red solid lines represent the lag-frequency spectra that also include positive propagating-fluctuation lags modelled as a power-law with different normalizations. Each circle locates the minimum point of each profile, showing that amplitude of the reverberation lag and the associating frequency at the minimum point can be affected by the propagating-fluctuation process leading to an uncertainty in determining their true values. Figure from Khanthasombat et al., 2024.

CURRICULUM VITAE

Name : Kamonwan Khanthasombat **Date of Birth** : 22/10/1998

Place of Birth : Rayong, Thailand

Residence : 222/33 Moo.4 (Village No.4), Maroeng Sub-district, Muang District, Nakhon Ratchasima 30000, Thailand

Tel : +66-918326529

Education

2017-2020 : Bachelor of Science, School of Physics, Institute of Science, Suranaree University of Technology

2020-present : Master of Science, School of Physics, Institute of Science, Suranaree University of Technology

Publication

1. **Khanthasombat, K.**, Chainakun, P., Young, A. J. (2023, in press). Parameter dependency on the public X-ray reverberation models KYNxilrev and KYNrefrev.
2. Ekprasert, J., Pongtharangkul, T., Chainakun, P., Fongkaew, I., **Khanthasombat, K.**, Kamngam, R., Boonsuan, W., Ditta, Z. M., Seemakram, W., and Boonlue, S. (2021). Kinetic model of a newly-isolated *Lysinibacillus* sp. strain YL and elastic properties of its biogenic Caco3 towards biocement application. Biotechnology Journal, 17(1). https://doi.org/10.1002/biot.202100124